Master's Thesis

석사 학위논문

A Power-Efficient μ-Heater Driving Circuit for Gas Sensor

Jonghyeok Park(박 종 혁 朴 鍾 爀)

Department of

Information and Communication Engineering

DGIST

2017

A Power-Efficient μ-Heater Driving Circuit for Gas Sensor

Advisor: Professor Junghyup Lee

Co-Advisor: Professor Minkyu Je

by

Jonghyeok Park

Department of Information and Communication Engineering

DGIST

A thesis submitted to the faculty of DGIST in partial fulfillment of the requirements for the degree of Master of Science in the Department of Information and Communication Engineering. The study was conducted in accordance with Code of Research Ethics[1].

November. 25. 2016

Approved by

Professor   Junghyup Lee   _____

(Advisor)

Professor   Minkyu Je   _____

(Co-Advisor)

A Power-Efficient μ-Heater Driving Circuit for Gas Sensor

Jonghyeok Park

Accepted in partial fulfillment of the requirements
for the degree of Master of Science

November. 25. 2016

Head of Committee _____(인)
                          Prof. Junghyup Lee
Committee Member _____(인)
                          Prof. Jae-eun Jang
Committee Member _____(인)
                          Prof. Minkyu Je

Abstract

Metal-oxide-semiconductor gas sensor consists of sensing layer detecting exposed gases and micro heater generating heat necessary for achieving the best performance of gas reaction. For gas sensor to get high sensitivity, optimal temperature of micro heater should be supplied to sensing layer. In addition, optimal temperature range of each micro heater has different characteristics based on sensing materials and target gases, which needs a demand for designing micro heater driving system. As a system driving circuit, Proportional-Integral(PI) controller and Pulse-Width Modulation(PWM) is used. PI controller plays a role for high accuracy and fast rising time of thermal transient response. PWM is used for low power consumption by adjusting pulse-width current heater current driving method rather than continuous current driving method. Continuous current driving method using current source consumes consistently, however PWM current driving method using switching transistor consumes only duty-on time, which can achieve higher thermal efficiency. Additionally, ADC interface block is designed for controlling ADC IC. In this thesis, a detail explanation of PI gain tuning method of PI controller will also be introduced for acquiring desired thermal transient response.

The driving circuit was implemented in Field-Programmable Gate Array(FPGA) using Altera Cyclone IV DE2-115 development, Altera Quartus II as logic synthesis and Mentographics Modelsim for RTL timing simulation. The gas sensor micro heater measured in this thesis is given by the laboratory of professor Jongbaeg Kim in mechanical engineering, Yonsei university.

Keywords: Gas sensor micro heater(hotplate), temperature control system, low power, Field-Programmable Gate Array(FPGA), PI controller

LIST OF CONTENTS

LIST OF TABLES

LIST OF FIGURES

I. INTRODUCTION

1.1 Motivation

The research and development of gas sensor interface have been consistently conducted since gas sensor was developed. Recently, the awareness of air pollution is being intensified due to modernization. Especially, air pollution of indoor environment is the issue of concern because indoor air quality is worsening gradually because of air pollutants, such as Particulate Matter(PM), Carbonyl Compounds, or Volatile Organic Compounds(VOCs). According to a research conducted by indoor air pollution and health effects in residential apartment in National Institute of Environmental Research(NIER) [1], the average indoor Particulate Matter(PM) concentration was higher than the safety standard level administrated by The World Health Organization(WHO). Each of total maximum PM-10 and PM-2.5 concentration in the house reached to 284ug/m^3 and 266ug/m^3, which can increases incidence rate of lung cancer indicated in figure1.1. Furthermore, Table1.2 shows that the indoor VOCs & Carbonyl Compounds concentration, such as Formaldehyde(HCHO), Toluene(C6H5CH3), and TVOC, was higher than the safety standard, which is detrimental for human respiratory system.

Table 1.1.

Particulate Matter(PM) environmental quality standard [Dimension : ug/m^3]

	PM-10		PM-2.5	
	A Day	**A Year**	**A Day**	**A Year**
The World Health Organization (WHO)	50	20	25	10
KOREA	100	50	50	25
CHINA	150	70	75	35
JAPAN	100	-	35	15
EU	50	40	-	25
USA	150	-	35	12~15
CANADA	25	-	15	-
AUSTRAILIA	50	-	25	8

PM-10
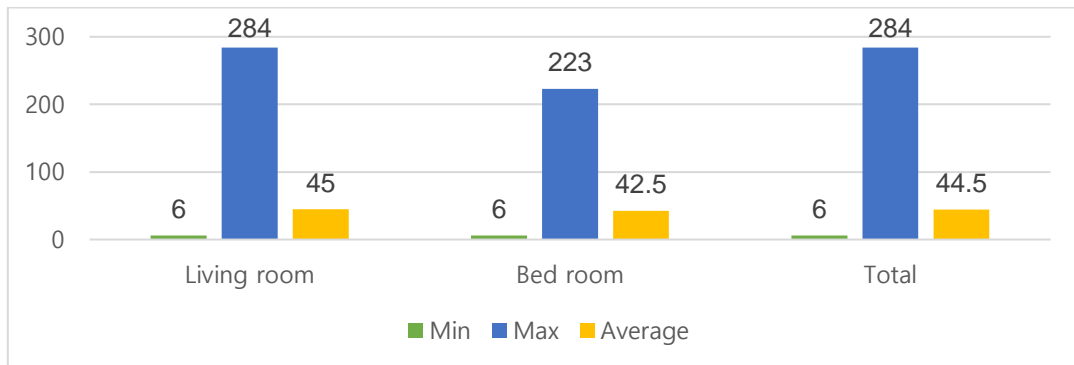
PM-2.5
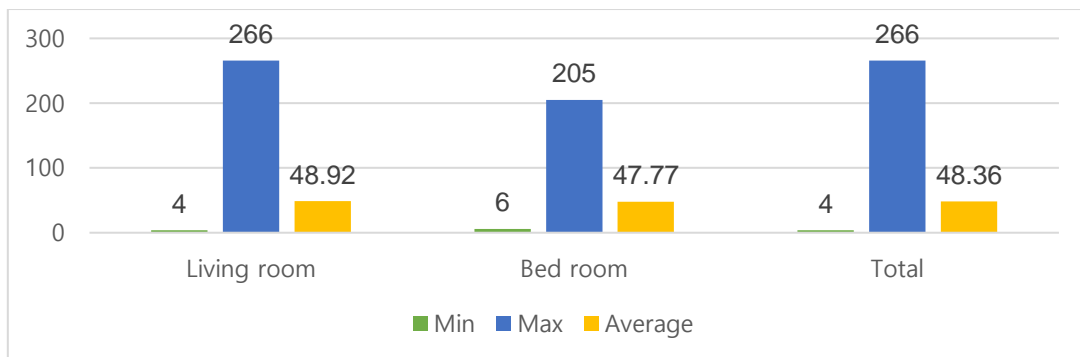
Figure 1.1. Indoor Particulate Matter(PM) concentration [Dimension : ug/m^3]

Table 1.2.

WHO environmental standard and Indoor quality for VOCs & Carbonyl Compounds
[Dimension : ug/m^3]

Volatile Compounds & Carbonyl Compounds	WHO standard	Indoor		
		Living room	Bed room	Total
Formaldehyde(HCHO)	30 ~ 120	127.03	132.91	129.97
Acetaldehyde(CH3CHO)	48	37.37	37.79	37.58
Xylene(C2H5CH=CH2)	870 ~ 1447	18.91	19.16	19.04
Ethylbenzene(C6H5CH2CH3)	1447 ~ 3880	10.30	10.49	10.39
Toluene(C6H5CH3)	260 ~ 1092	115.38	113.99	114.68
Styrene(C6H5CH=CH2)	30 ~ 300	9.34	10.20	9.77
TVOC	200 ~ 3000	635.63	667.42	651.52

As a result, alternatives are being suggested to avoid those detrimental gases One of them is to set up gas sensor platform using commercial gas sensors. There are various kinds of commercial gas sensors which senses particular gases. If gas sensors enable to sense harmful gases with high accuracy, the accidents or even risks for death can be prevented in advance by alarming the danger. However, the problem is that commercial gas sensors on sale does not have high sensitivity and selectivity upon to target gas. Therefore, there is a necessity to enhance the response of gas sensor and to find the characteristics related to gaseous reactivity. The gas sensor has a part of heater to help gas sensing. And the characteristic of gas sensitivity is highly dependent on the temperature of gas sensor heater. Each gas sensor has the range of heater temperature for optimal gas sensing and has different temperature range. It means that if there is a temperature control system for gas sensor, the gas sensor optimally senses with exposed gases, which can acknowledge gas concentration with high accuracy and even reduces harmful condition.

1.2 The Operating Principle of Gas Sensor

The metal-oxide-semiconductor(MOS) resistive gas sensors are one of the most widely investigated categories in gas sensors. Due to low costs for production, simplicity for use, and reliability, MOS gas sensors are commonly utilized in the field of gas sensing on air conditions. The fundamental operation of a gas response is the interaction of the gas with sensing layer material. The reaction is influenced by several internal and external factors: material characteristics, sensing area, and microstructure of sensing layer as an internal factor and temperature, humidity as an external factor. One of the important parameters related to gas response is sensitivity, which indicates how well a gas sensor reacts with exposed gases. Thus, much efforts have been conducted to improve the sensitivity of gas sensor.

To find methods to enhance the sensitivity, we need to look into the sensing mechanism of MOX gas sensor. The well-known sensing mechanism so far is electrons trapping at adsorbed molecules and energy band bending induced by charged molecules on the surface layer, which introduces the change of conductivity. The step of sensing mechanism is indicated in figure 1.2 [2]. When the metal oxide surface layer is heated with the operating temperature of 300~400℃ and O2 molecules in the air are adsorbed as O- on the surface of metal oxide sensing layer, they extract the electrons on the conductions band. The electron trapping contributes to the energy band bending and makes depletion region(Δgas) with no electron charge carriers and potential barrier($eV_{surface}$). With the lapse of time, the metal oxide surface is filled with O-, the adsorption of O2 molecules are stopped and ready for chemical reaction with exposed gases.
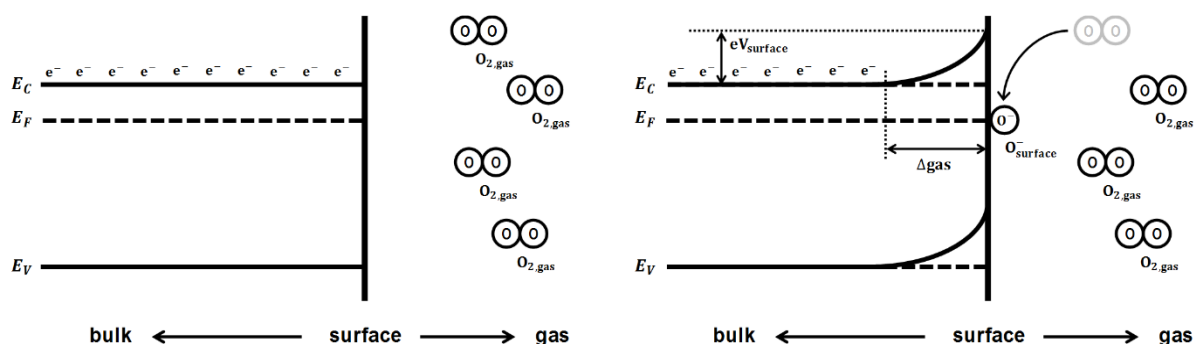
Figure 1.2 Energy band diagram before and after gas adsorption

The figure 1.3 shows the microstructure and energy band diagram of metal oxide surface conductive mechanism when carbon monoxide(CO) is exposed on the surface grains. CO gas molecules chemically react

4

with surface O- and release CO2 gas and electrons. The released electrons are carried to the bulk material of the grain. While the number of surface O- decreases, the thickness of depletion region decreases together. Then the potential barrier on the grain boundary is lowered and it leads to the increase of conductivity.
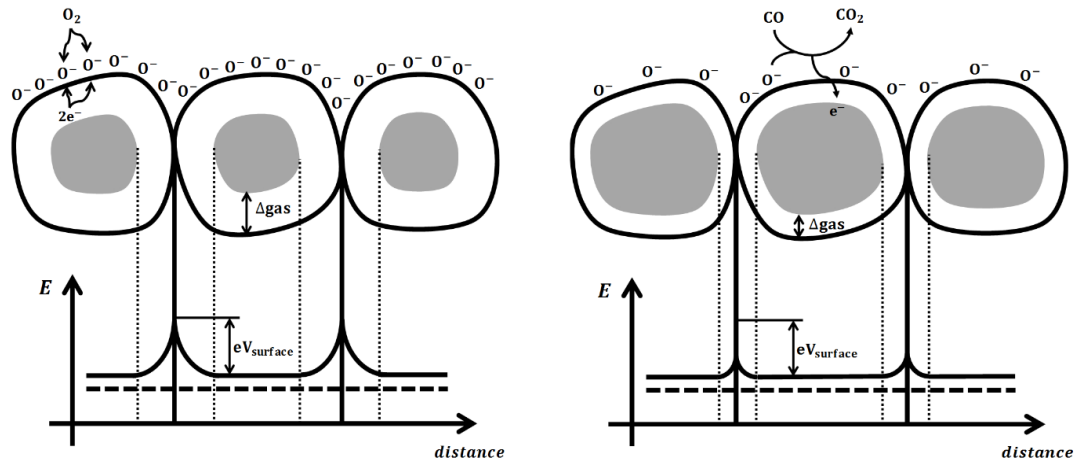
Figure 1.3. Microstructural and energy band diagram of metal oxide conductive mechanism

Until now, the sensing mechanism of metal oxide gas sensor was introduced to find the parameter for improving gas sensor sensitivity. As mention before, there were some internal and external factors related to sensitivity. Among those factors, one of controllable parameters is temperature. The temperature of the micro-hotplate inside the gas sensor is highly dependent on the sensor response and sensitivity. In addition, the optimal operating temperature is different on each gas sensor and each target gas. Therefore, temperature control system for gas sensor is necessary for allowing optimum gas sensor sensitivity to gases.

1.3 Previous Research of μ-Heater Driving Circuit for Gas Sensor

From now on, there has been increasing interest and continuing research about driving system for gas sensor μ-heater. Looking into research for μ-heater driving system, most of them was designed to satisfy the following specifications: high temperature accuracy and high thermal efficiency of heater. High thermal accuracy is

indispensable for precision temperature control when designing μ-heater driving system. If steady-state temperature of heater is not settled on target temperature, optimal operation of gas sensor cannot be achieved, which reduces the sensitivity and selectivity for target gas. Additionally, high thermal efficiency in μ-heater is important specifications for driving system. If thermal efficiency is high, μ-heater in gas sensor can increase its temperature higher as consuming less power. Reducing heater power consumption facilitates to the applications for the portable and hand-held instruments.

Now, I will introduce two general methods to control gas sensor μ-heater temperature. The principle that μ-heater can generate temperature is due to electrical power applied to heater. When the electrical voltage is applied to heater, electron charge carriers start to flow and they make the current through heater. Therefore, both of heater voltage and current makes power and it generates temperature of μ-heater (The detail principle will be discussed in the next chapter). Based on the principle, two methods are used for controlling temperature: one is continuous current driving method using current source and the other is on-off current driving method. Table 1.3 shows previous μ-heater driving system for gas sensor that overall characteristics and implementations are briefly introduced.

Table 1.3.

The previous research of gas sensor μ-heater driving system

	[3]	[4]	[5]
μ-heater current driving method	Continuous current driving method	Continuous current driving method	On-off current driving method
Main control circuits	P controller	PID control + DAC	On-off hysteresis
Steady-state error	$\neq 0$	0	$\neq 0$
Advantages	Simple structure	High temperature accuracy, Fast transient response	Simple structure
Disadvantages	Temperature offset error	Complex structure	Temperature variation

The suggested topology in [3] is implemented by negative feedback proportional controller using simple operational amplifier. Comparing the control voltage with the voltage measured by temperature sensor, the output

voltage proportional to the error is input to a power transistor. Figure 1.4 shows the circuit diagram of temperature proportional controller for micro hotplate.
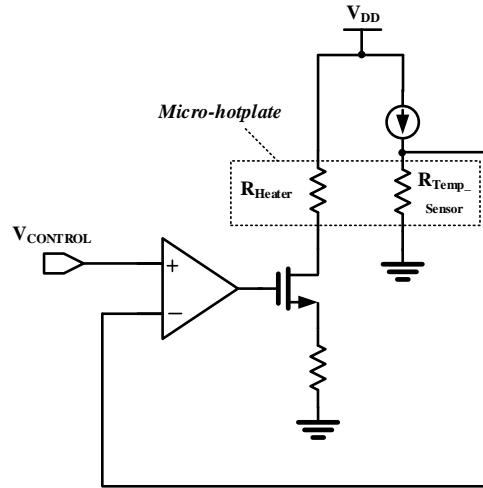
Figure 1.4. Circuit diagram of temperature proportional controller for micro hotplate

The micro-hotplate structure consists of a poly temperature sensor to detect the temperature of micro heater and a poly heater in micro-hotplate. Single-ended analog proportional heater temperature controller enables to control the operating temperature from room temperature to 400°C. An operational amplifier is applied to drive the power transistor. The power transistor provides the constant current flowing through the poly heater(R_{HEATER}) by controlling the gate-to-source voltage of MOS transistor. The voltage across the poly temperature sensor(R_{TEMP_SENSOR}) is fed back to the negative input of the operational amplifier. If the error between $V_{CONTROL}$ and the feedback voltage is large, the output voltage of op-amp and the amount of the current across heater resistor increase. On the other hand, the error is small, which means $V_{CONTROL}$ and the feedback voltage have small difference, the output voltage of op-amp and the amount of the current decrease. The principle advantage of this method is simple structure, small area consumption and low cost. However, the disadvantage is that the steady-state error of proportional temperature controller by the DC offset voltage of operational amplifier can make temperature offset error and reduce temperature accuracy.

The topology suggested in [4] is implemented by negative feedback proportional-integral-derivative (PID) temperature controller. Analogous to proportional control method, the error between set-point and feedback temperature is input to the heater adding integral and derivative term with error. The circuit diagram of temperature PID controller for micro-hotplate is shown in Figure 1.5.
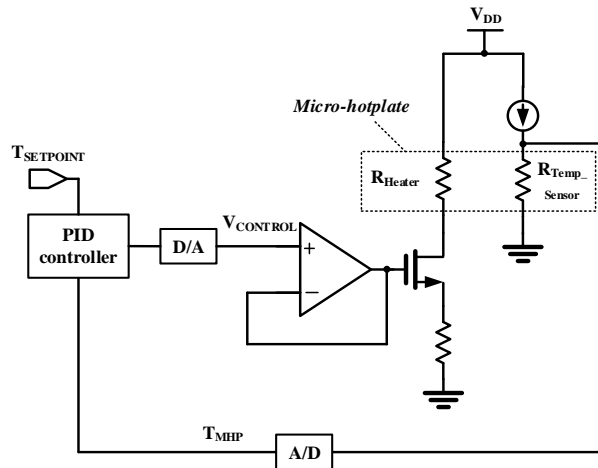
Figure 1.5. Circuit diagram of temperature PID controller for micro-hotplate

The micro-hotplate temperature (T_{MHP}) and the set-point temperature ($T_{SETPOINT}$) are input to a digital PID temperature controller. The digital output of the PID controller is converted to the analog voltage ($V_{CONTROL}$) by D/A converter and it is applied to a buffer. The output of the buffer drives the power transistor, which controls the current flowing through the heater resistor (R_{HEATER}). The temperature control method using PID controller is almost the same as using proportional control, however, PID controller is preferable because it has several benefits. Comparing proportional controller, PID controller has advantages of high thermal accuracy and minimum steady-state error compared to proportional control due to integral term. Also, additional derivative term can make the temperature transient response fast by reducing rising time or settling time. And PID controller contributes high stability to the system. However, the drawback of PID controller is that the structure is more complex than proportional controller and additional gain tuning techniques are necessary. The topology of [3] and [4] is using power transistor as a voltage-controlled current source. When DC voltage is applied to the transistor, the amount of the current is determined. In this case, the transistor is operated in saturation region when the drain-to-source current has almost constant value. If input voltage increases, the constant current also increases.

The approach shown in [5] is using an on-off controller to control the temperature of micro-hotplate. The digital on-off controller is one of the simplest structure. The micro-hotplate temperature is compared with set-point temperature at each sampling period. If the hotplate temperature is lower than set-point temperature, the maximum power, logically high, is applied to switching transistor, otherwise, no power, logically low, is applied. As indicated in figure 1.6, the temperature control method is similar to proportional control method [3] in regard that the feedback temperature is compared to the desired temperature. The difference is that by switching on and

8

off the transistor, the current across the heater flows or not, which increases or decreases heater power, whereas the methods [3], [4] apply continuous power to the heater. This is the advantage of on-off controller that on-off current driving method consumes lower power for μ-heater than continuous current driving method using current source [3], [4] (The detail explanation will be discussed in 1.4). In addition, on-off controller has simple structure to drive heater. However, the drawback is high temperature variation occurred by fast switching time. Fast on-off time leads to poor temperature accuracy and can damage the heater. In order to prevent the variation by fast switching, the on-off controller includes a hysteresis: a dead band, a region around the set-point which does not need control action in. Using hysteresis, the temperature variation problem can be reduced, however, it still difficult to achieve good stability.
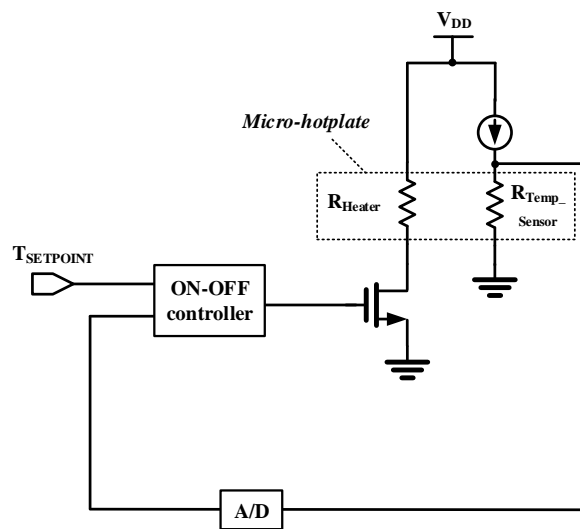
Figure 1.6. Circuit diagram of temperature On-Off controller for micro-hotplate

1.4 Design Considerations

The previous research of μ-heater driving circuits were designed to fulfill high thermal accuracy and low power consumption. To achieve accurate target temperature, PID controller in [4] is preferable than P controller or On-off controller due to additional integral and derivative term. However, the problem is that when continuous current driving method using current source is used such as [3], [4], it is difficult to acquire any power efficiency in driving μ-heater. This is the reason why on-off controller topology [5] is applied by on-off current driving method using switch.

Now, I will introduce about the detail explanation of two methods: continuous current driving method using current source and on-off current driving method using switch. Figure 1.7 shows the comparison of two current driving method for μ-heater.
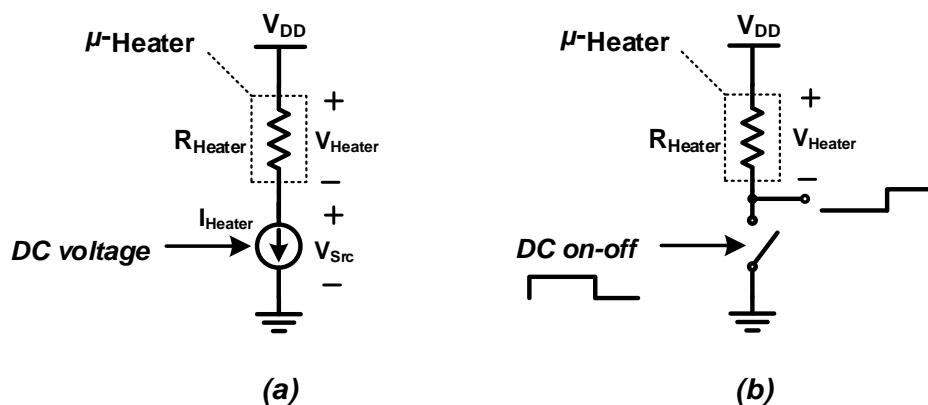
Figure 1.7 The comparison of two current driving method for μ-heater;

(a) continuous current driving method using current source   (b) on-off current driving method using switch

In figure 1.7 (a), the heater current(I_{Heater}) has constant value determined by DC input voltage-controlled current source. As changing DC input voltage of current source, the amount of current and the voltage across the heater(V_{Heater}) are determined, which leads to control heater power and temperature. The current source is implemented by MOS transistor in saturation region. It means that the voltage drop exists in current source and the power dissipated in current source should be considered when driving μ-heater. Therefore, the total power dissipation of heater in (a) can be represented by

$$\text{Total power}_{(a)} = I_{Heater} \cdot (V_{Heater} + V_{Src}) \tag{1}$$

In figure 1.7 (b), the heater current only flows when the switch turns on compared to (a) whose current always flows. The switch can be also implemented by MOS transistor in triode region. Therefore, the voltage drop across triode-region transistor is negligibly small and all the voltage is applied to heater. The total power consumption can be calculated by the maximum heater voltage(V_{DD}) and current($I_{Heater,VDD}$), and also it is highly dependent on turn-on duty ratio. As a result, the total power dissipation of heater in (b) can be represented by

$$\text{Total power}_{(b)} = I_{Heater,VDD} \cdot V_{DD} \cdot \left(\frac{turn-on\ time}{T}\right) \tag{2}$$

As mentioned above, the circuit topology in this thesis will choose on-off current control method (b) to reduce heater power consumption. However, the drawback of this method is high temperature variation seen as oscillated transient response, which leads to poor temperature accuracy and poor thermal stability. Therefore, to compensate the disadvantages of previous on-off controller topology, PI controller with pulse-width modulation(PWM) are proposed in this thesis. By changing on-off duty ratio proportional to input digital value, the average heater voltage and current are determined. PWM operates the same as DAC, however, the only difference is that PWM makes pulse signal and DAC makes continuous DC signal. It means that PWM method can reduce power consumption in driving heater as explained before. Figure 1.8 shows the proposed current driving method for μ-heater. Total power consumption is the same as the equation (2) that turn-on time of figure 1.8 indicates input signal duty-on time.
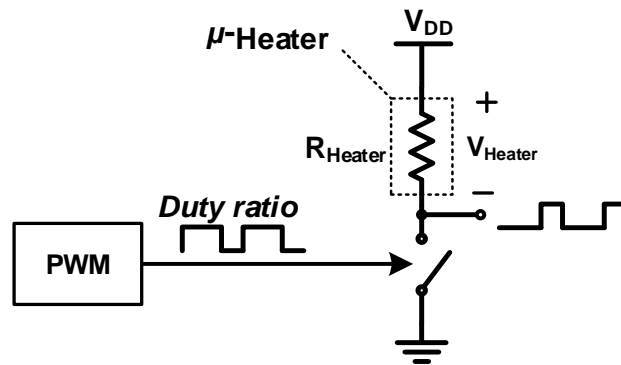
Figure 1.8 The proposed current driving method for μ-heater

In addition, the temperature variation problem of duty on-off control can be avoided by using PI controller. By using PI controller, the feedback heater temperature can follow the set-point temperature with high precision

and minimum steady-state error. The reason why PID controller is not implemented is that micro heater samples used in this thesis have small heat capacity, which means they inherently have a fast transient response. Thus, derivative term, performing to quicken the response, is avoided in the controller. Also, the derivative term is not used because it can have a possibility to exacerbate the temperature ripple problems. The whole block diagram of the proposed temperature control system is shown in figure 1.9.
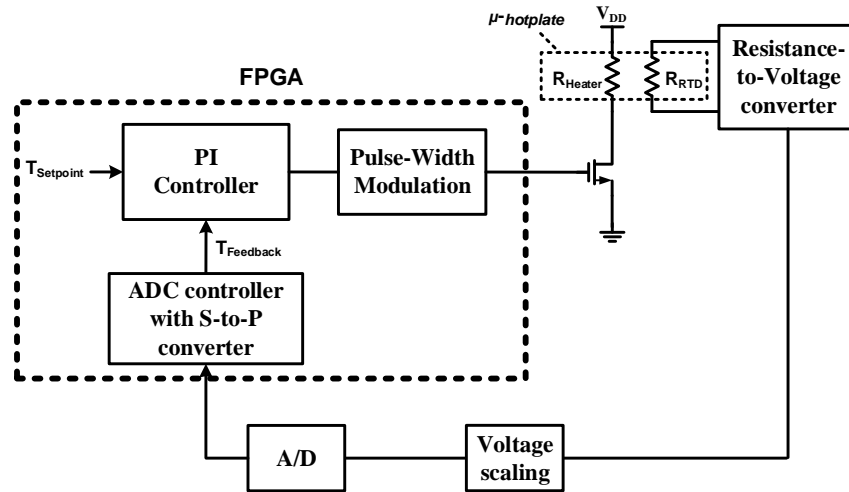
Figure 1.9 The whole block diagram of FPGA-based temperature control system

The whole system is implemented in PCB level, therefore, A/D, voltage scaling, and resistance-to-voltage converter block are used by commercial IC of several companies. The PI controller and PWM circuits are implemented using FPGA Altera Cyclone IV DE2-115 development board.

1.5 Thesis Organization

In chapter 2, the hardware modeling for micro heater and driving circuit will be introduced. As representing thermal operation of μ-heater theoretically, I will introduce the modeling of micro heater. In addition, the model of PI controller as a main circuit of μ-heater driving circuits will be represented. After we calculate the feedback-loop transfer function of the entire system in s-domain, the P, I gain tuning method will be presented in detail. The z-transform method will also be presented for FPGA implementation.

In chapter 3, FPGA-implemented micro heater driving circuits will be introduced. The internal architecture and detail implementation of each FPGA module will be explained.

In chapter 4, the simulation results of each FPGA module will be introduced to verify their proper operation. And their simulation result will be also compared with actual measurement result after downloading to the FPGA board.

In chapter 5, the conclusion and further studies of this thesis will be introduced.

I. Hardware Modeling for Micro Heater Driving System

As a main circuit for driving gas sensor micro heater, PI control and PWM method are proposed in this thesis. The overall system has a structure of negative feedback. Therefore, there is a need to obtain a closed-loop transfer function by mathematically modeling each system blocks to interpret how the whole system works. In this chapter, the mathematical modeling for micro heater is introduced, and the overall architecture and P, I gain tuning method of PI controller are dealt with.

1.1 Thermal Model for Micro Heater

As introduced before, high temperature heating is an important issue for the performance of MOX gas sensor. This heat can be acquired by Joule heat generation in a heating element. If the current flows to the heating element, or a conductor, myriads of electrons migrate through the conductor. They make a current density in the conductor, where Joule heat is generated. This is called Joule heat generation. The density of Joule heat has a characteristic of non-uniform distribution, which leads to a localized hotspot; high degree of heat is generated in the spot of high current density and low degree of heat is in the spot of low current density. Therefore, theses hot spots occurred by Joule heat introduce large temperature gradient causing a heat transfer to other materials.

When electrical power is applied to the hotplate, Joule heat is generated and this heat is transferred to other materials, which leads to heat loss. Based on Joule heat generation, thermal model of micro heater can be expressed as follows [6] [7]:

$$\begin{bmatrix} \text{The rate of energy} \\ \text{stored in hotplate} \end{bmatrix} = \begin{bmatrix} \text{The net rate of energy} \\ \text{into or out of hotplate} \end{bmatrix} + \begin{bmatrix} \text{The rate of energy} \\ \text{generated by hotplate} \end{bmatrix} \quad (1)$$

The rate of energy stored is the heat storage depending on the density and heat capacity of the hotplate. The net rate of energy is heat transfer depending on thermal conductivity of the hotplate. And the heat generation is the system input power. In practice, the performance of the heat transfer is different according to several parameters, such as structure's material, dimension, layer density etc. Also, the transfer of heat into and out of the hotplate can be classified into three mechanisms: heat conduction to the other materials surrounding micro hotplate, heat convection to the air, radiation. However, the thermal transient response can be simply obtained by approximating actual three mechanisms of temperature distribution inside the sensor and expressing the thermal behavior with thermal resistance R_{th} and thermal capacitance C_{th}. If the electrical power applied to the hotplate is P_{el}, equation (1) can be described the following equation:

$$C_{th}\frac{dT}{dt} = -\frac{T-T_0}{R_{th}} + P_{el} \quad (2)$$

Rewriting the equation (2) expressing $\Delta T = T - T_0$, the derivative term in the left side term can be described $\frac{d\Delta T}{dt}$ because T_0 is constant. The equation (2) and can be solved using Laplace analysis. The temperature transient response to a step function of electrical power is given by

$$\Delta T(s) = \frac{K}{RCs+1}P_{el}(s) \quad (3)$$

$$\Delta T(t) = K\left(1 - e^{-1/\tau}\right)P_{el}(s), \ \tau = R_{th}C_{th} \quad (4)$$

where K is the magnitude of input power, and τ is thermal time constant expressed with thermal resistance and thermal capacitance. The equation (3) is indicated in s-domain and the equation (4) in time domain. As shown in these two equations, the thermal dynamics of the hotplate are modeled by a first-order differential equation whose dynamics are the same as first-order low pass filter RC circuit.

In this thesis, selected micro heaters used for measurement are given from the laboratory of professor Jongbaeg Kim in mechanical engineering, Yonsei university. The time constant τ of the selected micro heater is 2.4msec, and K is 92.85 that the temperature is 350°C when 3.5V is applied to the heater.

1.2 PI controller

In the thesis, PI controller is proposed as a temperature control circuit for micro heater. It will be introduced about the method for tuning P, I gain to meet transient specifications and the design of PI controller. The PI algorithm consists of two basic terms as proportional term and integral term. The basic form of PI control algorithm is given by

$$u(t) = K_p e(t) + K_i \int_0^t e(\tau)d\tau \tag{5}$$

where K_p, K_i is a proportional and integral gain, $e(t)$ is the error signal, and $u(t)$ is the control input. The PI control equation (5) is given in frequency s-domain using Laplace transform by

$$U(s) = \left(K_p + \frac{K_i}{s} \right) E(s) \tag{6}$$

To interpret the operation of the whole system depending on PI controller, it is necessary to figure out the closed-loop transfer function in s-domain. Including the equation (6), the block diagram of temperature control system in s-domain is shown in figure 2.1.
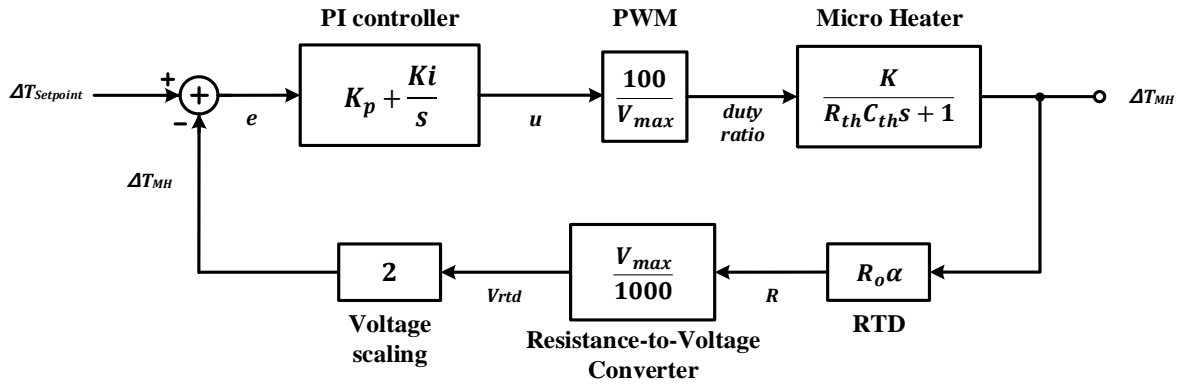
Figure 2.1 Block diagram of micro heater temperature control system in s-domain

In figure 2.1, PI controller and micro heater system block is explained before. $\Delta T_{setpoint}$ is the setpoint temperature and ΔT_{MH} is the micro heater temperature. V_{max} [V] denotes the operating voltage of the system, whose value is 4.0V. $\frac{100}{V_{max}}$ is PWM system block that converts the control input u to *duty ratio* [%]. $R_o\alpha$ is resistance-temperature detector (RTD), whose equation is $R = R_o(1 + \alpha\Delta T)$ omitting R_o, R_o is base resistance at room temperature and α is temperature coefficient [1/°C]. RTD converts temperature of a heating element into resistance and is located inside the sensor near the heating element. $\frac{V_{max}}{1000}$ is a system block of commercial integrated chip MAX6603 manufactured by MAXIM, which converts RTD resistance into voltage. And the voltage scaling block plays a role of extending the range of V_{rtd} because RTD resistance variation range is not high. It is implemented by non-inverting amp using MCP609 of Microchip Technology. From the s-domain block diagram in figure 2.1, the closed-loop transfer function is achieved by

$$\frac{\Delta T_{MH}}{\Delta T_{setpoint}} = \frac{25K(K_p s + K_i)}{R_{th}C_{th}s^2 + (1 + 25K \cdot K_p)s + 25K \cdot K_i} \tag{7}$$

The equation of closed-loop transfer function (7) has a characteristic of a second-order system response. Compared to the simplicity of a first-order micro heater system, the second-order system exhibits various responses. Whereas varying a first-order system's parameter simply changes the speed of the response, a second-order system's parameter can change several forms of the response. For example, the second-order system can display damped, underdamped, or oscillated form of its transient response, whose forms are determined by system poles. By placing the location of the system poles, it is available to intuitively judge the system's transient form without the need for sketching the response [8], [9].

17

Before interpret and make the desired transient response for the equation (7), three fundamental concepts are needed for the ensuing discussion: (1) Natural frequency ω_n and damping ratio ζ (2) Rising time T_r, Settling time T_s, Peak time T_p, the percent overshoot $\%OS$ (3) Root locus

(1) Natural frequency ω_n and damping ratio ζ

These two parameters are physically meaningful for second-order system. Natural frequency is the frequency of oscillation of the system without damping. Damping ratio is the degree the transient envelope decays. The equation can be defined by the ratio of the exponential decay frequency of the envelop to the natural frequency. They can be used to describe and analyze the characteristics of the second-order transient response.

(2) Rising time T_r, Settling time T_s, Peak time T_p, the percent overshoot $\%OS$

There are four important transient specifications of the step input. These information lets us know the transient response form, such as damping form, underdamped form, and how fast the transient changes. They are defined as follows:

- *Rising time T_r* : The time required for the waveform to go from 0.1 of the final value to 0.9 of the final value.

- *Settling time T_s* : The time required for the transient's damped oscillations to reach and stay within 2% of the steady-state value.

- *Peak time T_p* : The time required to reach the first, or maximum peak.

- *Percent overshoot $\%OS$* : The amount that the waveform overshoots the steady-state, or final value at the peak time.

These four specifications are inferred from the general second-order transfer function. Using natural frequency and damping ratio defined before, the general second-order transfer function $G(s)$ can be represented by

$$G(s) = \frac{\omega_n^2}{s^2 + 2\zeta\omega_n s + \omega_n^2} \tag{8}$$

Calculating the step response for the equation (8), the transform of the response $C(s)$ is given by

$$C(s) = \frac{\omega_n{}^2}{s(s^2+2\zeta\omega_n s+\omega_n{}^2)} \tag{9}$$

Taking the inverse Laplace transform of $C(s)$, it is represented by

$$c(t) = 1 - \frac{1}{\sqrt{1-\zeta^2}} e^{-\zeta\omega_n t} \cos((\omega_n\sqrt{1-\zeta^2})t - \theta) \tag{10}$$

From the equation (10), the result of hand-calculation of the transient specifications is as follows:

$$T_s = \frac{4}{\zeta\omega_n} \tag{11}$$

$$T_p = \frac{\pi}{\omega_n\sqrt{1-\zeta^2}} \tag{12}$$

$$\%OS = e^{-\zeta\pi \big/ \sqrt{1-\zeta^2}} \times 100 \tag{13}$$

A precise analytical relationship between rising time with natural frequency and damping ratio cannot be found.

(3) Root locus

Root locus, a graphical presentation of the closed-loop poles as a system parameter is varied, is a powerful method of analysis and design for both transient response and the stability. The root locus typically allows us to choose the proper loop gain and the closed-loop pole location to meet transient response specifications, whose specifications is to improve transient response, steady-state error, and stability.

Now, let us analyze the closed-loop transfer function of equation (7). In the equation (7), there are two poles determined by PI controller gain, and the system response can have different transient characteristics according to the gain. The steps of PI controller gain tuning method using root locus are as follows:

1. Choose the desired transient response specifications (T_s, T_p, $\%OS$).

2. Calculate natural frequency ω_n and damping ratio ζ, and find the desired pole location of the closed-loop system to meet transient specifications.

3. Find the location of PI controller zero K_i/K_p using the open-loop poles.

4. Draw root locus combining the poles and zeros of PI controller and plant. On the locus, find the loop gain K_p at the desired pole, which indicates the proportional gain, and compare simulation and hand-calculation whether the transient specifications are met.

5. If both of the results are almost the same each other, find the integral gain K_i from K_i/K_p.

The desired transient specification: rising time < 10sec, steady-state error $\approx$ 0, Phase margin > 45deg. The rising time less than 10 second is based on the time micro hotplate temperature reaches on target temperature and surrounded oxygen molecules are completely adsorbed on the sensing surface. The time for the sensor used in the thesis takes about 90 ~ 100 seconds, thus the rising time specifications was put on one to ten of that time. However, the faster rising time reaches on target temperature, the better performance is. Therefore, let us make the transient response as fast as possible. And the steady-state error is almost zero means the heater temperature can follow the desired temperature with high accuracy. Even though the steady-state error does not become zero in practical, the minimum error is better. Finally, the system phase margin (PM) was designed to have larger than 45 degrees. If the system phase margin is larger than 45 degrees, the system can be stable and the output transient response does not oscillate or diverge. Generally, additional margin about 45 to 60 or 70 degrees is common target specification for the system.

If PM is larger than 45 degrees, the transient response shows a critical or overdamped characteristic. Therefore, let us design the transient have almost zero percent of overshoot based on steady-state value. Also, the settling time is set to 5msec to make the rising time as fast as possible. From the equation (13), the damping ratio (ζ) has 0.9465 when %OS is almost 0 percent from the equation (13). And natural frequency ω_n has 845.22 from the settling time equation (11). Then, the location of the desired pole, or dominant pole, of the second-order transfer function can be achieved from the figure 2.2 shown below.
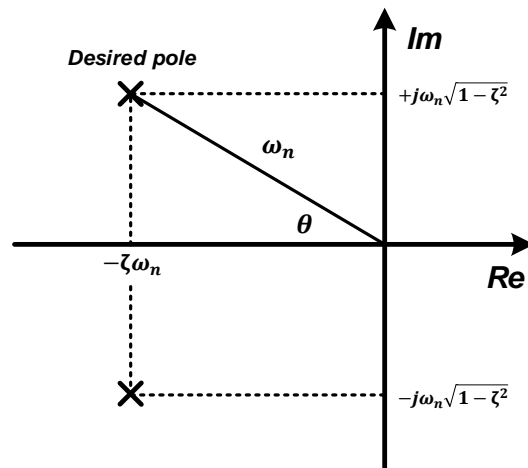
Figure 2.2 Dominant pole plot for second-order system

From the figure 2.2, the desired pole is -800 + j272.76. The next step is to achieve the controller zero Z_C. Using the geometry shown in figure 2.3, the controller zero's location can be calculated.
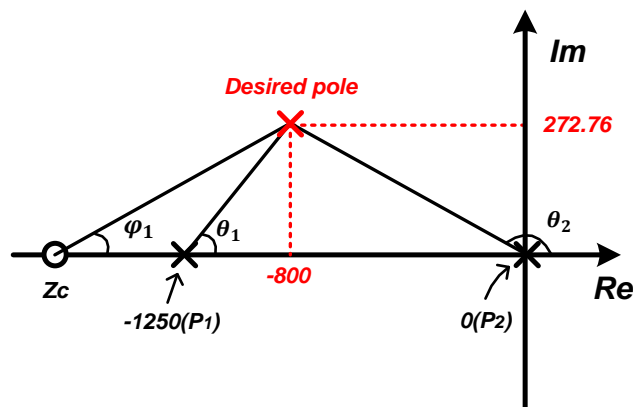
Figure 2.3 Calculation of PI controller zero location

$$\theta_1 = \tan^{-1}\left(\frac{272.76}{1250 - 800}\right) \approx 31.22°$$

$$\theta_2 = 180° - \tan^{-1}\left(\frac{272.76}{800}\right) \approx 161.17°$$

$$\varphi_1 = \theta_1 + \theta_2 - 180° \approx 12.39°$$

$$|Z_C| = \frac{272.76}{\tan \varphi_1} + 800 \approx 2041.62$$

From the figure 2.3, the controller zero Z_C is 2041.62. And now, drawing the root locus for the poles of the controller and the plant, the loop gain K_p, proportional gain of PI controller, can be achieved when the closed-loop pole is at the desired pole. The figure 2.4 shows the root locus for PI compensated micro heater system.
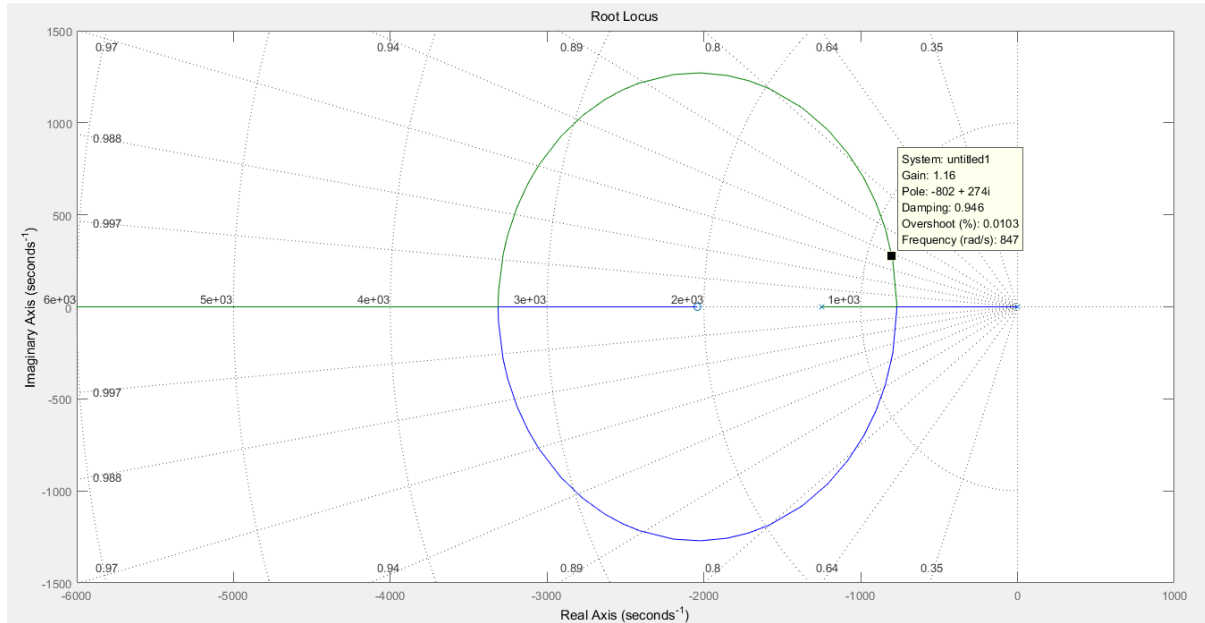
Figure 2.4 Root locus for Micro heater model with PI controller

As shown in figure 2.4, the loop gain K_p is 1.16. And the integral gain K_i can be achieved from the controller zero $Z_C (= K_i/K_p)$, which is 2368.28.

Until now, the PI controller gain tuning is done. Finally, There is a need for us to verify the output temperature transient response whether the transient specifications of %OS and T_s is met for the desired specifications. Using these P and I gain (K_p, K_i) in PI controller, the transient response simulation result is shown in figure 2.5 The result is simulated in Simulink model.
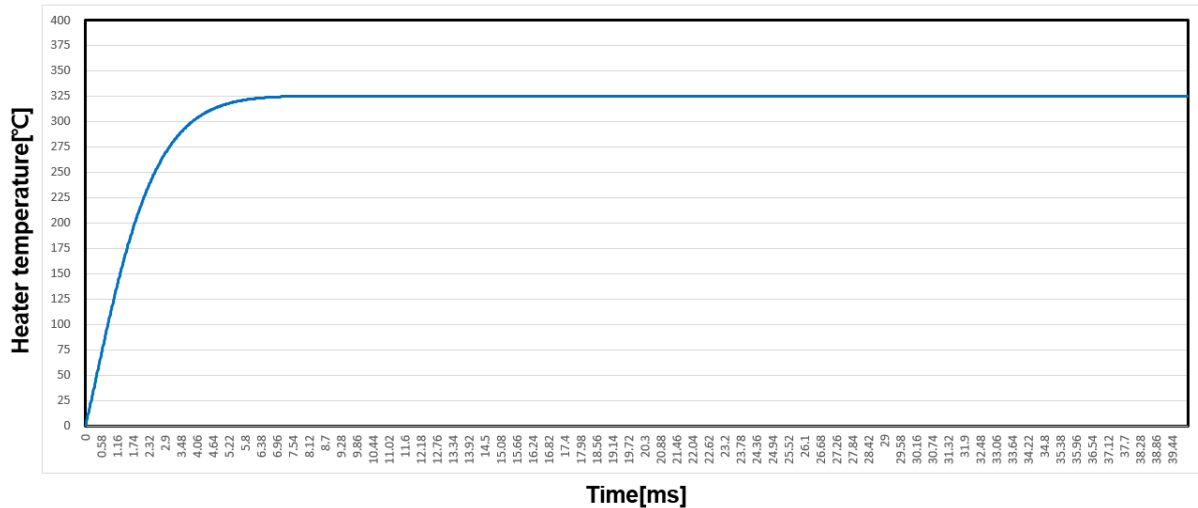
Figure 2.5 Simulation result of thermal transient response in Simulink

Based on the transient results of figure 2.5, %OS is about 0.03% and T_r is 3.3msec and T_s is 5.4msec, whose simulation results are similar to the desired specifications. Table 2.1 summarizes the comparison with hand calculated result and simulation result in the overall progress.

Table 2.1.

The comparison of hand-calculation and simulation results

	PI control	
	Calculation	Simulation
(Controller x Plant) Transfer function	$K\dfrac{(s + 2041.62)}{s} \times \dfrac{123.5}{(0.8 \times 10^{-3}s + 1)}$	
Dominant poles	s = -800 $\pm$ j272.76	s = -802 $\pm$ j274
Loop gain(K)	2.15	
Damping ratio(ζ)	0.9465	0.9460
Natural frequency(ω_n)	845.22	385.92
%Overshoot	0%	0.01%
Rise time(T_r)	3msec	3.3msec
Settling time(T_s)	5msec	5.4msec
Steady-state error	0	0
Controller Gain	K_p = 1.16, K_i = 2368.28	
Phase Margin	50.2 degree	

The both results are also similar each other, which means design verifications are reasonable. And the s-domain PI controller transfer function $C(s)$ is represented by

23

$$C(s) = \frac{1.16(s+2041.62)}{s} \tag{14}$$

For implementing PI controller design using FPGA, there is a need to transform the expression of analog domain to digital domain. In digital domain, the value is updated at each sampling period. In discretizing continuous PI controller, the transformation of integral term in PI controller is significant. There are three methods to transform continuous integral term into discrete term: Forward Euler method, Backward Euler method, and Tustin or Bilinear method. To figure out the difference among them, it is necessary to get into a bit of mathematics for analysis. Let us understand an example shown in figure 2.6. The integrator output is defined by y and the input by u. The current sample is T_k and the previous T_{k-1}. And the sampling period is T_s $(= T_k - T_{k-1})$.
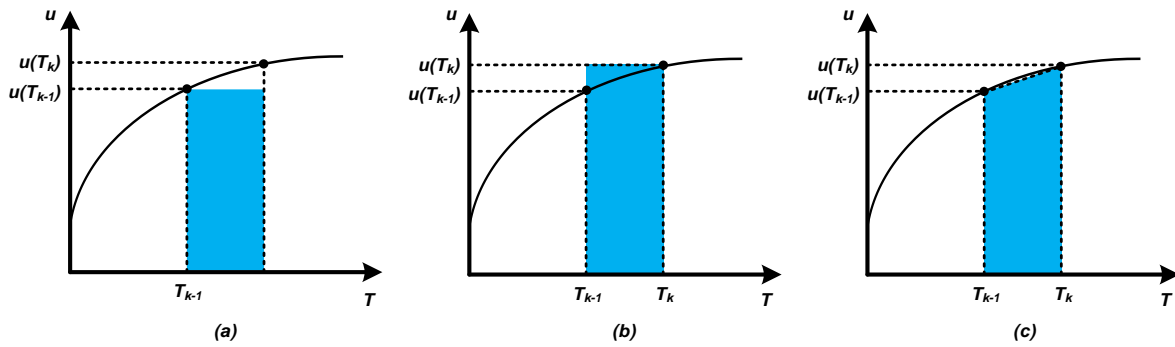
Figure 2.6 The discretization methods for integral term:

(a) Forward Euler method (b) Backward Euler method (c) Tustin or Bilinear method

$$y(k) = y(k-1) + T_s \cdot u(T_{k-1}) \tag{15}$$

$$y(k) = y(k-1) + T_s \cdot u(T_k) \tag{16}$$

$$y(k) = y(k-1) + T_s \cdot \frac{u(T_{k-1})+u(T_k)}{2} \tag{17}$$

Forward Euler method is defined by the equation (15). This means that the current output is computed as the previous sample output added to the previous input times the sampling period T_s. Backward Euler method is defined by the equation (16), where the output is dependent on the current input value. In the Tustin or Bilinear method in the equation (17), the output is dependent on the average of the previous and current input samples.

In the thesis, Tustin method is used for discretizing continuous time-domain PI controller. In the equation (6), continuous time-domain PI controller was represented in frequency s-domain. In order to design

controller in digital domain, z-transform should be applied to it. From the equation (17), the method of z-transform using Tustin method is shown below.

$$y[z] = z^{-1}y[z] + \frac{T_S}{2} \cdot \left[z^{-1}u[z] + u[z] \right]$$

$$(1 - z^{-1}) \cdot y[z] = y[z] + \frac{T_S}{2} \cdot (1 + z^{-1}) \cdot u[z]$$

$$\frac{y[z]}{u[z]} = \frac{T_S}{2} \cdot \frac{(1+z^{-1})}{(1-z^{-1})} = \frac{T_S}{2} \cdot \frac{(Z+1)}{(z-1)}$$

$$s = \frac{T_S}{2} \cdot \frac{(Z+1)}{(z-1)} \tag{18}$$

,where T_s denotes the sampling period.

Before using the equation (18) for transforming PI controller, let us determine appropriate sampling period T_s considering the whole system. In general case, as the sampling period gets smaller (higher sampling rate), the designed digital controller's output yields a closer match to the analog output. However, if the sampling rate is very high, it can increase the operating power consumption and damage the micro heater due to fast switching transition. Thus, proper sampling rate should be considered. To determine the sampling frequency, the output transient response for the step input at each different frequency is shown in the figure 2.7.
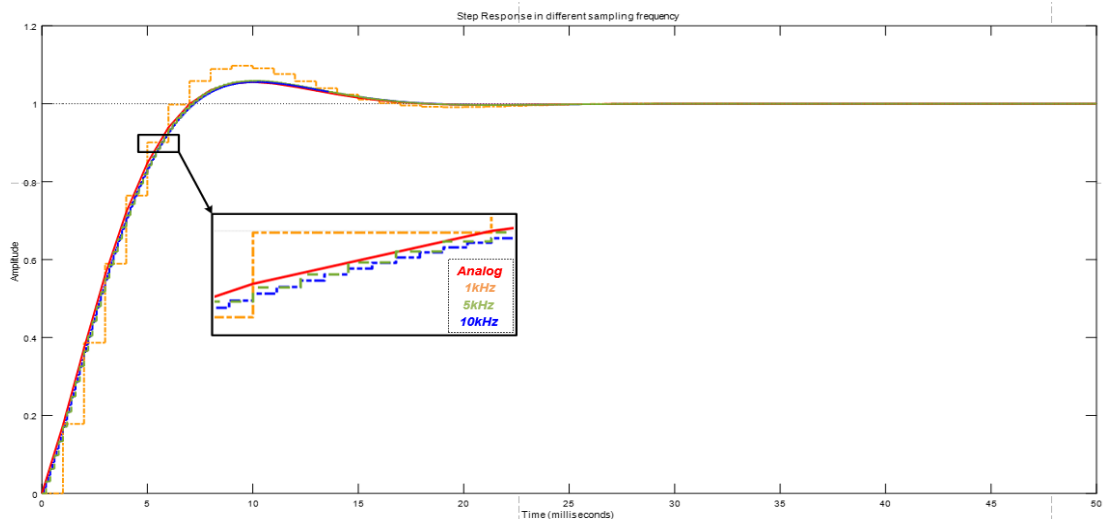
Figure 2.7 Step response in different sampling frequency:

Analog(red), 1kHz(orange), 5kHz(green), 10kHz(blue)

As shown in the figure 2.7, 10kHz(0.0001sec) sampling frequency(period) was chosen for the system operating frequency.

25

Now, using the equation (18) and sampling period of 10KHz, the z-domain transfer function of PI controller is represented by

$$C[z] = \frac{U[z]}{E[z]} = \frac{1.1021(Z-0.8147)}{(z-1)} \qquad (19)$$

,where $E[z]$ and $U[z]$ is input and output of PI controller represented in z-domain. And the equation (19) is transformed into discrete time-domain equation represented by

$$u[k] = u[k - T_s] + K_{pz} \cdot e[k] - K_{iz} \cdot e[k - T_s] \qquad (20)$$

,where $e[k]$ is the current error signal, $e[k - T_s]$ is the previous error signal and $u[k]$ is the control signal, $u[k - T_s]$ is the previous integral signal. The coefficients K_{pz} and K_{iz} are discrete P gain and I gain given in (21) and (22).

$$K_{pz} = K_p + K_i \cdot \frac{T_s}{2} \qquad (21)$$

$$K_{iz} = -K_p + K_i \cdot \frac{T_s}{2} \qquad (22)$$

,where K_p and K_i is continuous P gain and I gain, that each of them is 1.16 and 2368.28. Using (21) and (22), K_{pz} and K_{iz} is 1.2784 and -1.0416. In summary, the whole system block diagram with s-domain blocks and z-domain PI controller is shown in the figure 2.8.
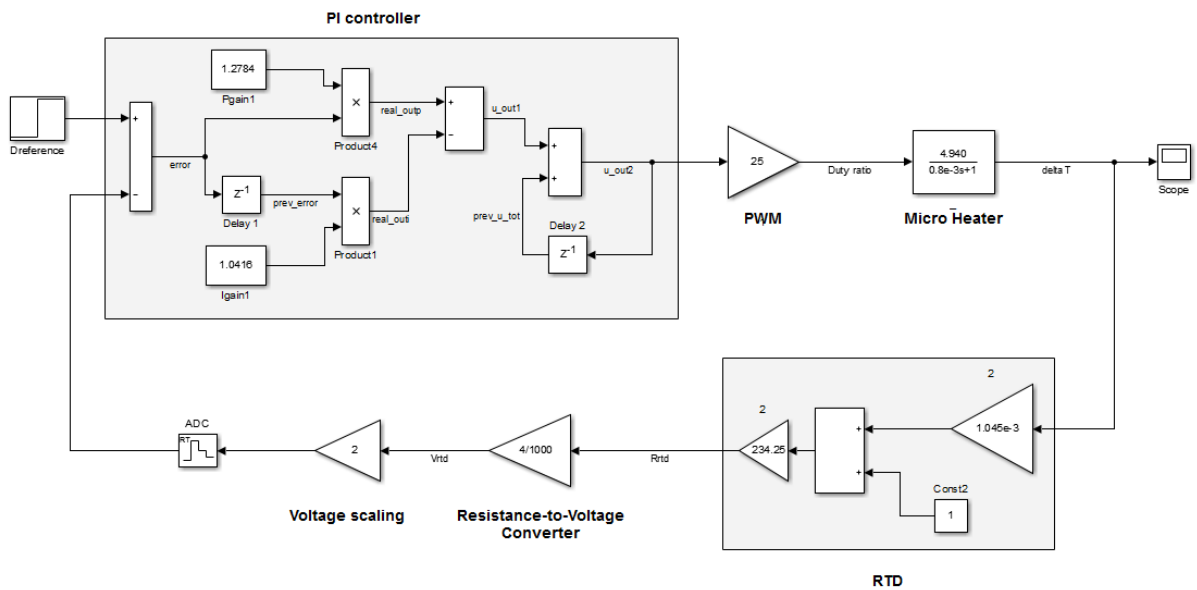
Figure 2.8 Block diagram of temperature control system in s-domain and z-domain

26

PI controller, PWM blocks in figure 2.8 are implemented using FPGA and the details will be introduced in the next chapter.

III. FPGA Implementation of Micro Heater Driving Circuit

As mentioned before, the micro heater driving circuits are implemented using FPGA. In FPGA implementation, PI controller, PWM as a main circuit, and Serial-to-Parallel converter were additionally designed. In this chapter, the detail implementation of them will be dealt with. In the thesis, Altera Cyclone IV DE2-115 development board was used as a FPGA hardware, Altera Quartus and Mentographics Modelsim as software tools. Quartus tools is for gate logic synthesis on FPGA chip and Modelsim is for Resistor Transistor Level (RTL) simulation of the circuits.

3.1 PI controller

In chapter 2.2, PI controller represented by discrete time domain and frequency z-domain equation was introduced to implement it using FPGA, whose result was the equation (20). In this section, FPGA implementation of PI controller will be introduced. The first step is to model the architecture of digital PI controller from (20). As shown in figure 2.7, the commercial IC of ADC, *ADC101S101* is used in the system, which has high speed and low power 10bit converter with maximum 1.25 MHz sampling rate. It converts an analog voltage to a digital value.

Due to the resolution of ADC, the input and output resolution of digital PI controller have also 10bit, decimal scale from 0 to 1023. The operating clock of PI controller is 10kHz as mentioned in figure 2.6. Based on this information, the internal architecture of PI controller can be designed as the figure 3.1 [10].
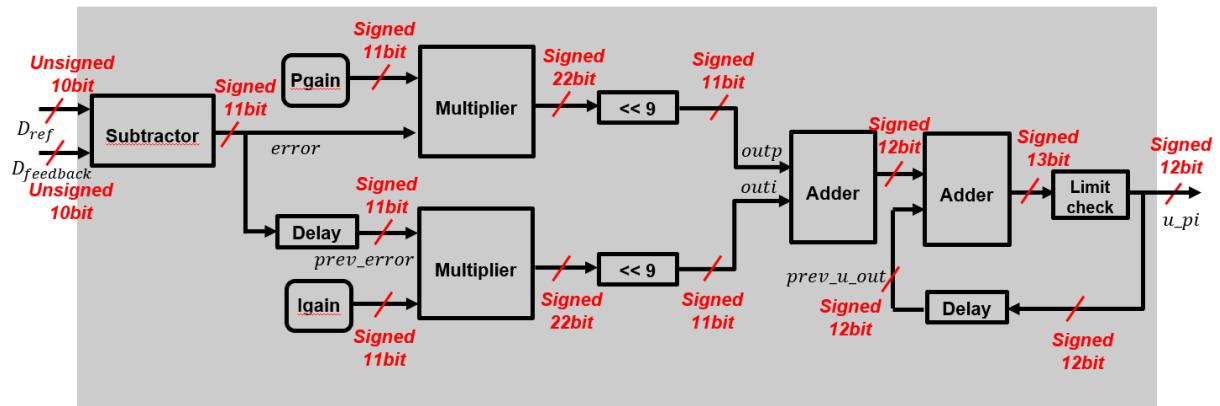
Figure 3.1 The architecture of digital PI controller

The architecture consists of two multipliers, two adders and one subtractor, and two delay blocks. Shifting 9bits (<<9) block after two multipliers is added due to P gain and I gain. P gain and I gain in z-domain (K_{pz}, K_{iz}) were 1.2784 and -1.0416. They are so small that the magnitude should be increased to avoid gain scale error. Therefore, the method used in this architecture is that two to the nine(2^9) is multiplied to P gain and I gain before getting into multipliers, and the multiplied decimals are shifted 9bit to the right, which means dividing 2^9 from the output decimals.

3.2 PWM (Pulse Width Modulation)

The principle of PWM is that the output voltage level varies depending on the pulse width. PWM module will generate a pulse waveform with appropriate duty cycle. The pulse signal of PWM is generated by comparing reference voltage with sawtooth wave of constant amplitude and frequency, which means comparator and counter is needed to make pulse signal. The 10bit counter is used to generate sawtooth signal, which counts the decimal values from 0 (00000_00000)₂ to maximum 1000 (11111_01000)₂. When counter reaches to

maximum value 1000, it returns to 0 and repeat it. The duty cycle has the range of $0 \leq \text{Duty} \leq \frac{1000}{1023} (\approx 97.76\%)$.

At each clock cycle, comparator compares the output of PI controller. The block diagram of PWM module is shown in figure 3.2. If D_{in} is higher than D_{ref}, comparator gives logic '1', otherwise it gives logic '0'. The operating clock of PWM (CLK_PWM) depends on total counting number and system clock. The PWM clock is 10MHz calculated by the equation (23) [11].

$$CLK\_PWM = System\ clock\ \times Total\ counting\ number = 10kHz \times 1000 = 10MHz \qquad (23)$$
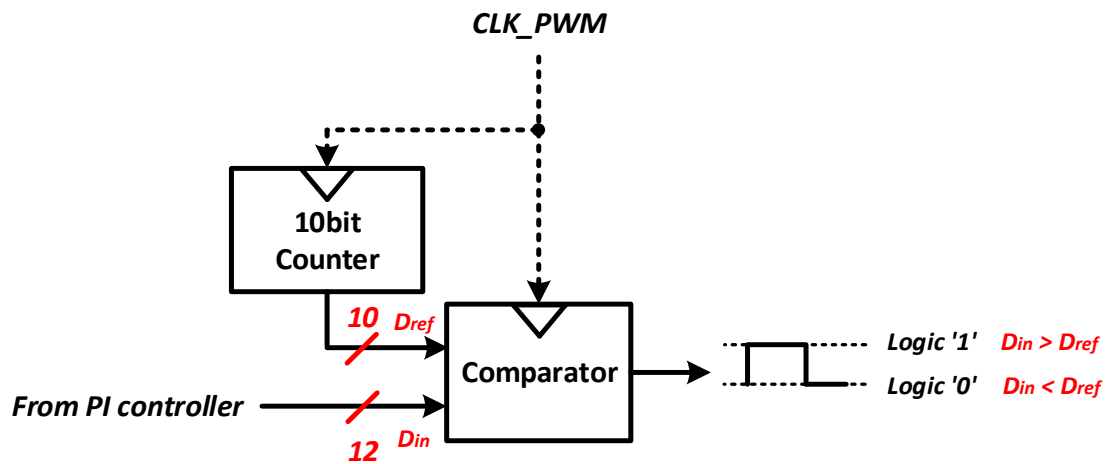
Figure 3.2 The block diagram of PWM module

3.3 ADC controller with Serial-to-Parallel converter

Serial-to-Parallel converter performs to convert a continuous serial digital data into parallel bus data. For commercial ADC chip, *ADC101S101* of 10bit digital converter is used in the system. Its operation is based on SPI communication protocol. Indicated in the datasheet [12], ADC operation depends on chip select clock *CSb* and using *SCLK* as synchronous clock, serial data bits are generated from *Serial_Dout* bit by bit. When performing a conversion, ADC IC reads the analog signal and converts it to a digital output. There are three lines connected with Serial-to-Parallel converter module in FPGA, and these lines are used to allow SPI communication between

ADC and the module. The figure 3.3 shows the interface of ADC controller with Serial-to-Parallel converter with ADC IC in FPGA.
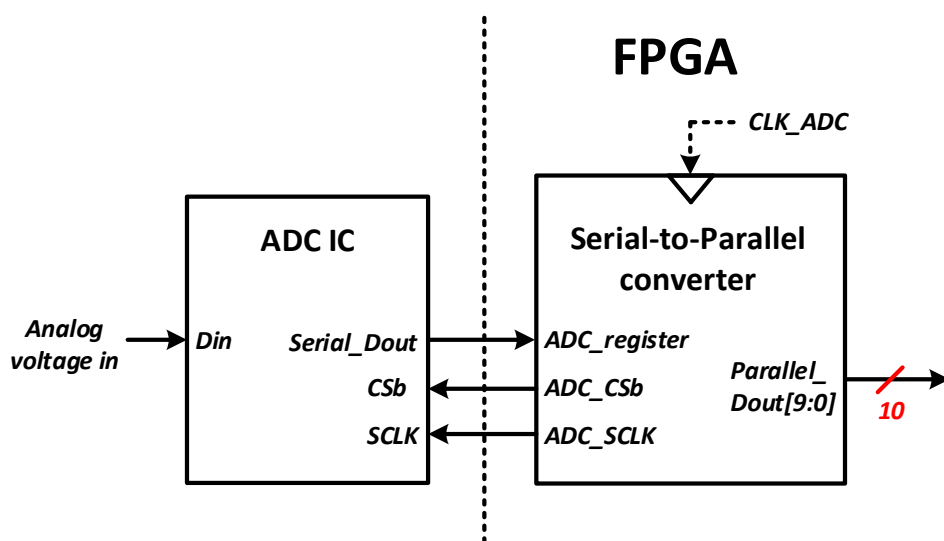
Figure 3.3 The interface of ADC controller with Serial-to-Parallel converter with ADC IC
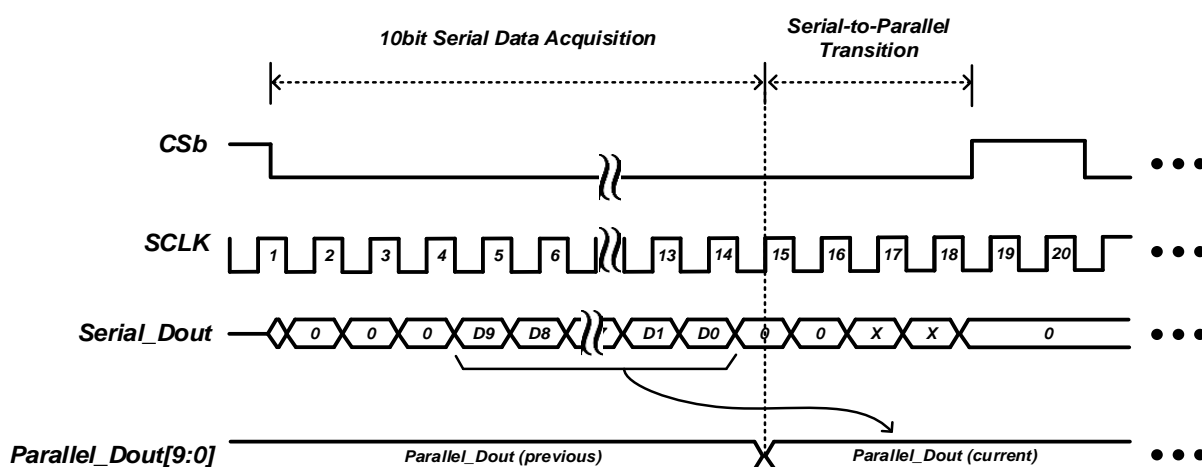
Figure 3.4 The timing diagram of ADC controller with Serial-to-Parallel converter interface

And the figure 3.4 shows the timing diagram of ADC controller with Serial-to-Parallel converter interface. The cycle starts with the falling edge of *CSb*. With the falling edge of *CSb*, the input signal is sampled and the conversion process is initiated. The ADC converts to serial bit at each negative edge. For the first four negative edges, the data word contains three or four leading zeros, followed by 10bit data from MSB to LSB and padded by 2 lagging zeros. During 10bit serial data acquisition time, the ADC stores 10bit serial data bit by bit.

At that time, the *Parallel_Dout* stores previously acquired digital value. As soon as the acquisition time is finished, ADC starts to transit serial 10bit to a parallel bit (bus)

In summary, the micro heater temperature control circuits in FPGA are composed of three modules: PI controller, PWM, and Serial-to-Parallel converter. The figure 3.5 shows these hardware modules and I/O pin assignments of FPGA-based temperature controller.
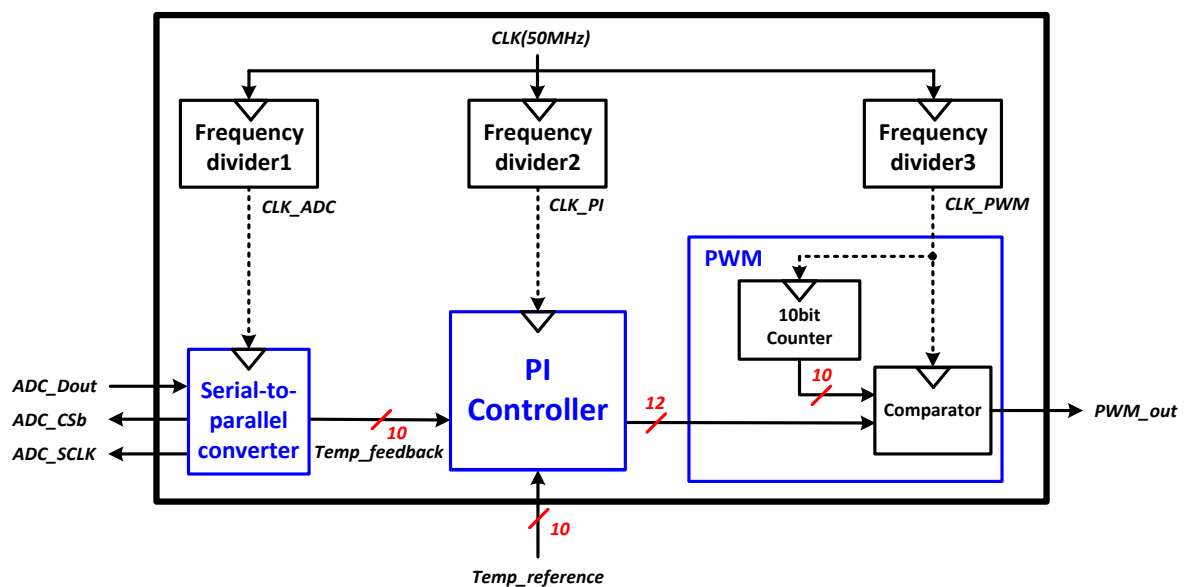
Figure 3.5 Hardware modules and I/O pin assignments of FPGA-based temperature controller

,where $Temp\_reference$ is the reference digital value, and $Temp\_reference$ is feedback digital value acquired from Serial-to-Parallel converter. These two values will be processed in PI controller and the output of PI controller will compare with 10bit counter leading proper pulse cycle. The original clock is 50MHz generated from embedded crystal oscillator in FPGA development board and three frequency dividers divide the original clock into three different clock CLK_ADC, CLK_PI, and CLK_PWM, operating clocks of these three modules.

IV. Measurement

In this chapter, the simulation results of FPGA-implemented modules (PI controller, PWM, and Serial-to-Parallel converter) and the actual measurement result of their FPGA hardware will be introduced. First, RTL level simulation will be conducted. After RTL simulation and downloading in FPGA board, we will confirm whether the actual operation and simulation result is the same or not. Especially, to verify the operation of FPGA PI controller based on figure 3.1, the ideal model is coded using MATLAB and this will be compared with its FPGA model. Finally, by testing feedback loop of the whole system including FPGA modules, driving commercial IC circuits, and micro heater, we will confirm that a feedback temperature can follow a desired temperature with desired transient specifications.

4.1 FPGA modules test

4.1.1 PI controller module test

As shown in figure 3.1, PI controller is composed of several modules, such as two multipliers, two adders, one subtractor, and two delays. Before we design PI controller based on the architecture of figure 3.1, it is necessary to confirm that the architecture properly works. Therefore, there should be an ideal model for FPGA

model verification. The ideal model is coded using MATLAB. The measurement setup is shown in figure 4.1 and the comparison result of these two model is in figure 4.2
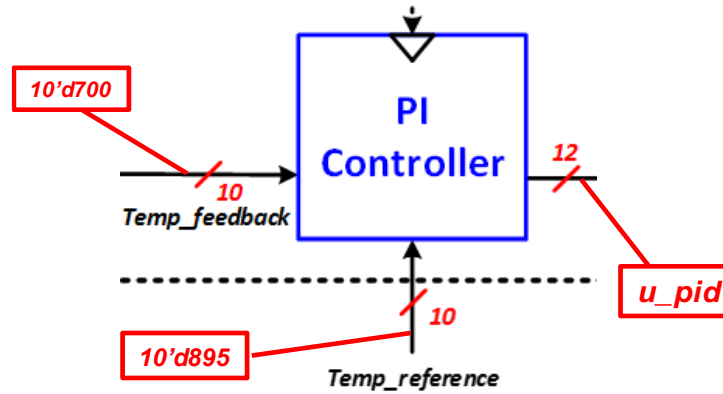
Figure 4.1 PI controller module measurement setup

Temp_reference and *Temp_feedback* are the input and *u_pid* is the output of PI controller We will fix *Temp_reference* to 10bit fixed integer value of 895 and *Temp_feedback* to 700, and simulate *u_pid* at each sampling period.

temp_reference	895	895	895	895	895	895	895	895	895	895
temp_feedback	700	700	700	700	700	700	700	700	700	700
error	195	195	195	195	195	195	195	195	195	195
prev_error	0	195	195	195	195	195	195	195	195	195
outp	115245	115245	115245	115245	115245	115245	115245	115245	115245	115245
outi	0	100620	100620	100620	100620	100620	100620	100620	100620	100620
real_outp	225	225	225	225	225	225	225	225	225	225
real_outi	0	196	196	196	196	196	196	196	196	196
u_out1	225	29	29	29	29	29	29	29	29	29
u_out2	225	254	283	312	341	370	399	428	457	486
prev_u_out2	0	225	254	283	312	341	370	399	428	457
u_pid	225	254	283	312	341	370	399	428	457	486

(a)
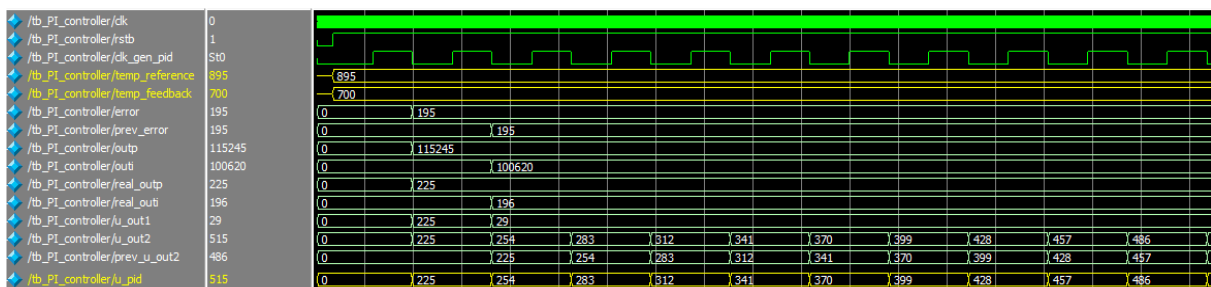
(b)

Figure 4.2 PI controller module measurement result:

(a) MATLAB ideal model data (b) FPGA model data

34

As you see measurement results of (a) and (b) for the same inputs, the output *u_pid* has the same result. However, the number of comparison groups are just 10 which can be small, thus we need to put more samples to be compared. Therefore, there are additional simulation with the same measurement setup, whose number of samples are 200 shown in figure 4.3
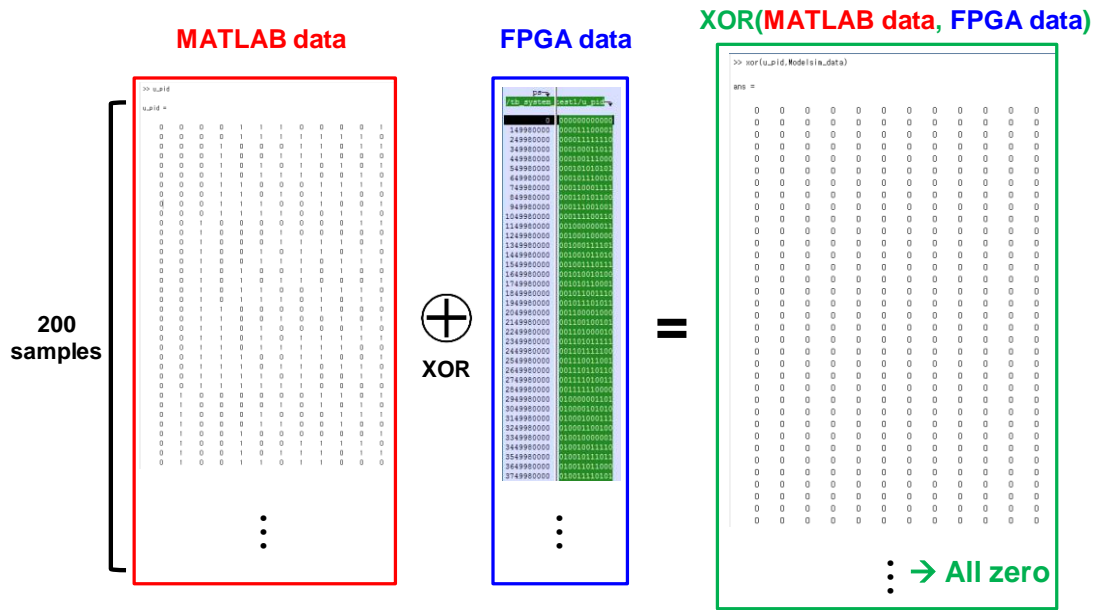
Figure 4.3 PI controller module measurement result (Tested for 200 samples)

To compare two logic value, general method is using XOR operation. When two logic values are the same, the results of their XOR operation is logic '0', otherwise logic '1'. The simulation result of MATLAB ideal model and FPGA model test for 200 samples is in green box. All of these logic values are zero, which means these two models are perfectly the same. Therefore, the verification of FPGA PI controller model is done.

4.1.2 PWM module test

As shown in figure 3.2, PWM module consists of 10bit counter and comparator. Actually, 10bit counter is 1000 counter which counts decimal 0 to 999. This is because if the counter counts decimal 1024, the PWM operating frequency is not integer value and it results a clock synchronization error. The measurement setup of PWM module is shown in figure 4.4.
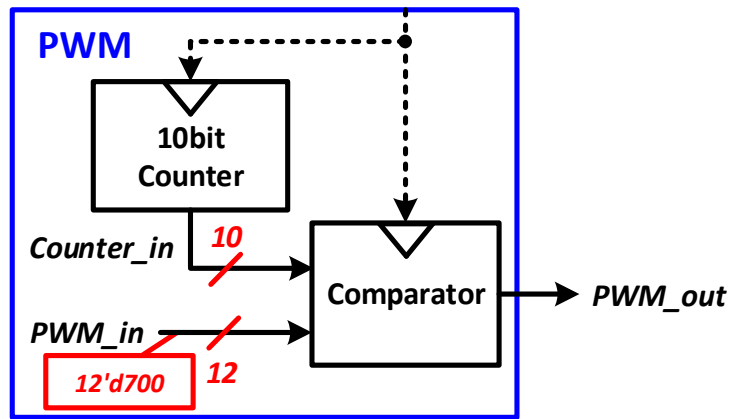
Figure 4.4 PWM module measurement setup

The input of comparator *PWM_in* is 12bit fixed integer value of 700. Counter_in is the output of 10bit counter, which counts up decimal 0 to 999 at each clock cycle and goes into comparator. When *PWM_in* is higher than *counter_in*, *PWM_out* results logic high, however lower than *counter_in*, *PWM_out* results logic low. . The simulation results of the PWM output is given in figure 4.5.
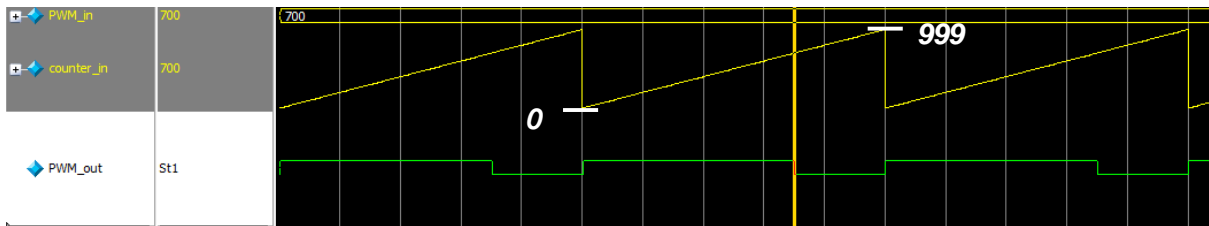
Figure 4.5 PWM module measurement result

4.1.3 ADC controller with Serial-to-Parallel converter module test

The measurement setup of Serial-to-Parallel converter module is the same as figure 3.3. The input analog voltage changes from 0 to 4V at 0.1V step and the 10bit output *Parallel_Dout* of the converter module is measured. The output measurement results of Serial-to-Parallel converter is shown in figure 4.6
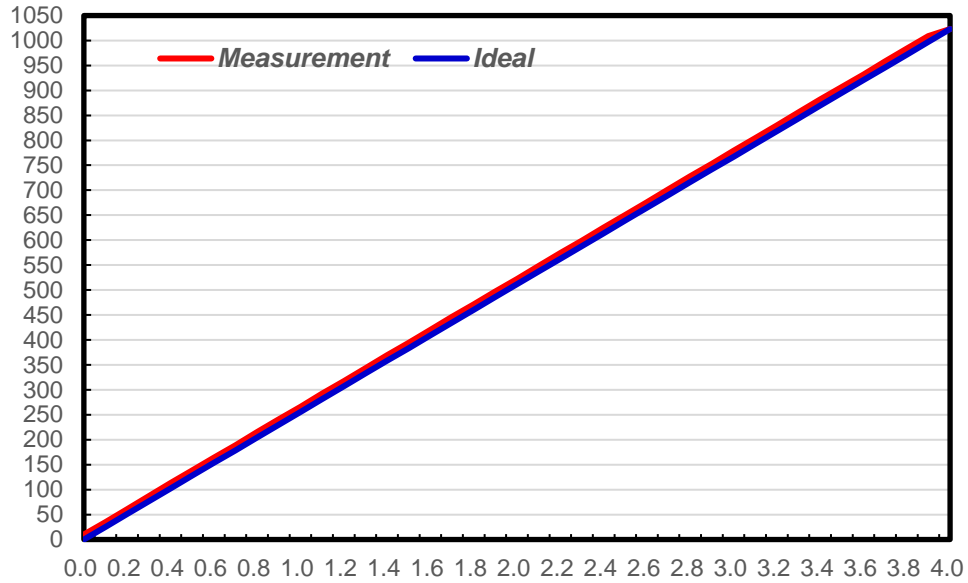
Figure 4.6 ADC controller with Serial-to-Parallel converter module measurement result

The blue line is the ideal decimal value corresponded to analog voltage and the red line is measurement decimal value of *Parallel_Dout*. The measurement value was a little higher than the ideal one, whose average error has +11 in decimal value.

4.2 Feedback loop test

In this section, we will perform feedback loop test for several micro heaters with FPGA-implemented circuits. The block diagram of hardware feedback loop was already introduced in figure 1.7. The test was performed using the total 7 micro heater given from the laboratory of professor Jongbaeg Kim in mechanical engineering, Yonsei university. Even though each RTDs were processed with similar characteristics, they have different characteristics of baseline resistance at room temperature Ro, temperature coefficient α, thermal time constant τ $(=R_{th}C_{th})$, and dc gain K due to process variation. The RTD characteristics of each sensor are summarized in table 4.1.

Table 4.1 RTD characteristics of each μ-heater sensor

	Ro [Ω]	α [1/°C]	τ $(=R_{th}C_{th})$ [sec]	K
Sensor #1	234.25	1.045e-3	0.80e-3	4.940
Sensor #2	231.52	0.918e-3	0.62e-3	4.074
Sensor #3	232.40	1.096e-3	0.77e-3	4.618
Sensor #4	234.03	1.063e-3	0.84e-3	4.422
Sensor #5	233.73	1.193e-3	0.78e-3	4.511
Sensor #6	242.7	1.193e-3	0.78e-3	4.329

Ro : baseline resistance at R.T   α : temperature coefficient of resistor
τ : thermal time constant K : heater dc gain

As shown in table 4.1, sensor #1, 3, 4, 5 have almost the same characteristics, however, sensor #2, 6, 7 seem to definitely different characteristics.

Before we confirm that each heater sensor has desired transient response with desired transient specifications, the proper operation of FPGA PI controller is sure to be tested using actual micro heater hardware. Therefore, we measured the tendency of thermal transient response by varying P gain and I gain of PI controller and confirmed whether the tendency is fitted to simulation results. The first test is testing the tendency of critical-damped transient response varying P gain with fixed I gain. The result is shown in figure 4.7.
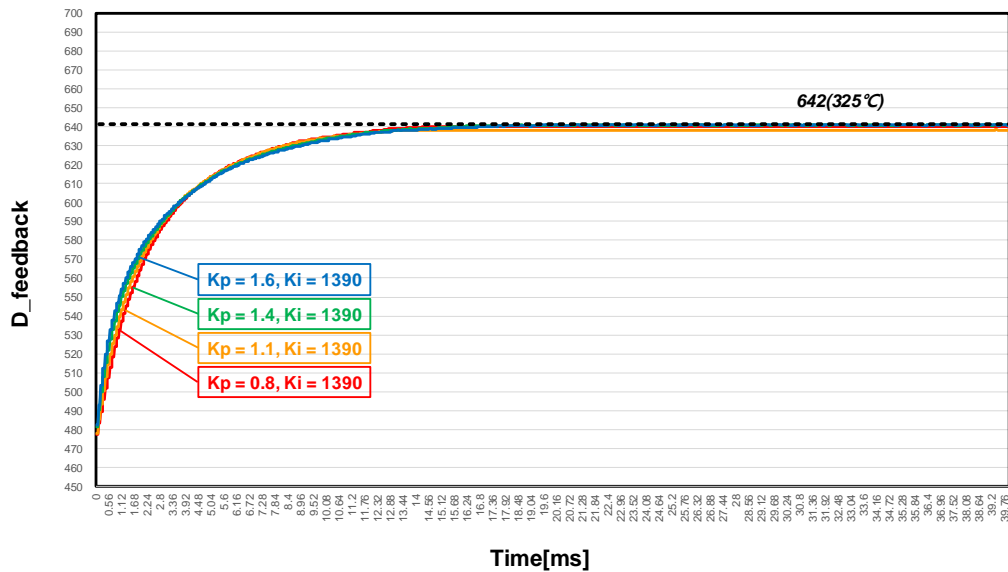
Figure 4.7 The tendency of thermal transient response (K_p varies and K_i constant)

When a set-point digital value is 642, the same as 325℃, a feedback digital value D_feedback is following the set-point value with critical-damped transient response. At that time, varying P gain of controller, we confirmed the tendency of the response. The increase of P gain means the increase of open loop gain proportional to error, which leads to the decrease of rising time. As shown in the figure 4.7, the rising time gradually decreases as P gain increases, and faster transient response can be achieved.

The second test is testing the tendency of under-damped transient response varying I gain with fixed P gain. The result is shown in figure 4.8.
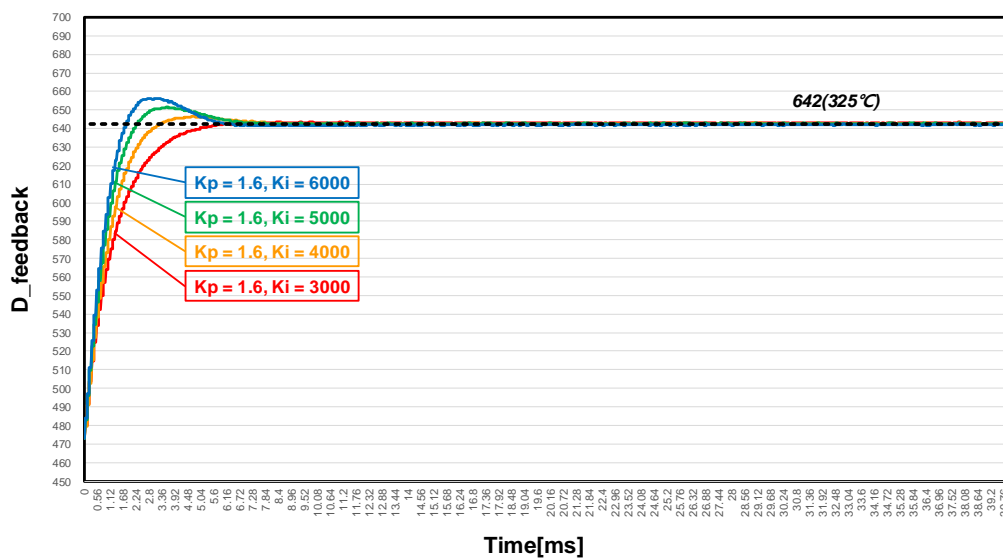
Figure 4.8 The tendency of thermal transient response (K_p constant and K_i varies)

The increase of I gain means the increase of open loop zero, which leads to the decrease of damping ratio and the increase of overshoot. The increase of overshoot corresponds to the decrease of rising time. As shown in the figure 4.8, the percentage of overshoot increases and the rising time decreases due to the increase of I gain. In summary of the test for transient response changing P gain and I gain, the transient tendency is the same as the simulation results, which means that PI controller properly operates with actual μ-heater hardware.

Now, let us look into thermal transient response matched to the desired specifications. The desired specification was that the rising time T_r is about 3ms, the settling time T_s is about 5ms, the percentage of overshoot is almost zero, and phase margin is larger than 45 degree. I acquired P, I gain corresponded to this

transient specification and the figure 4.9 shows the measurement results of thermal transient response for actual µ-heater.
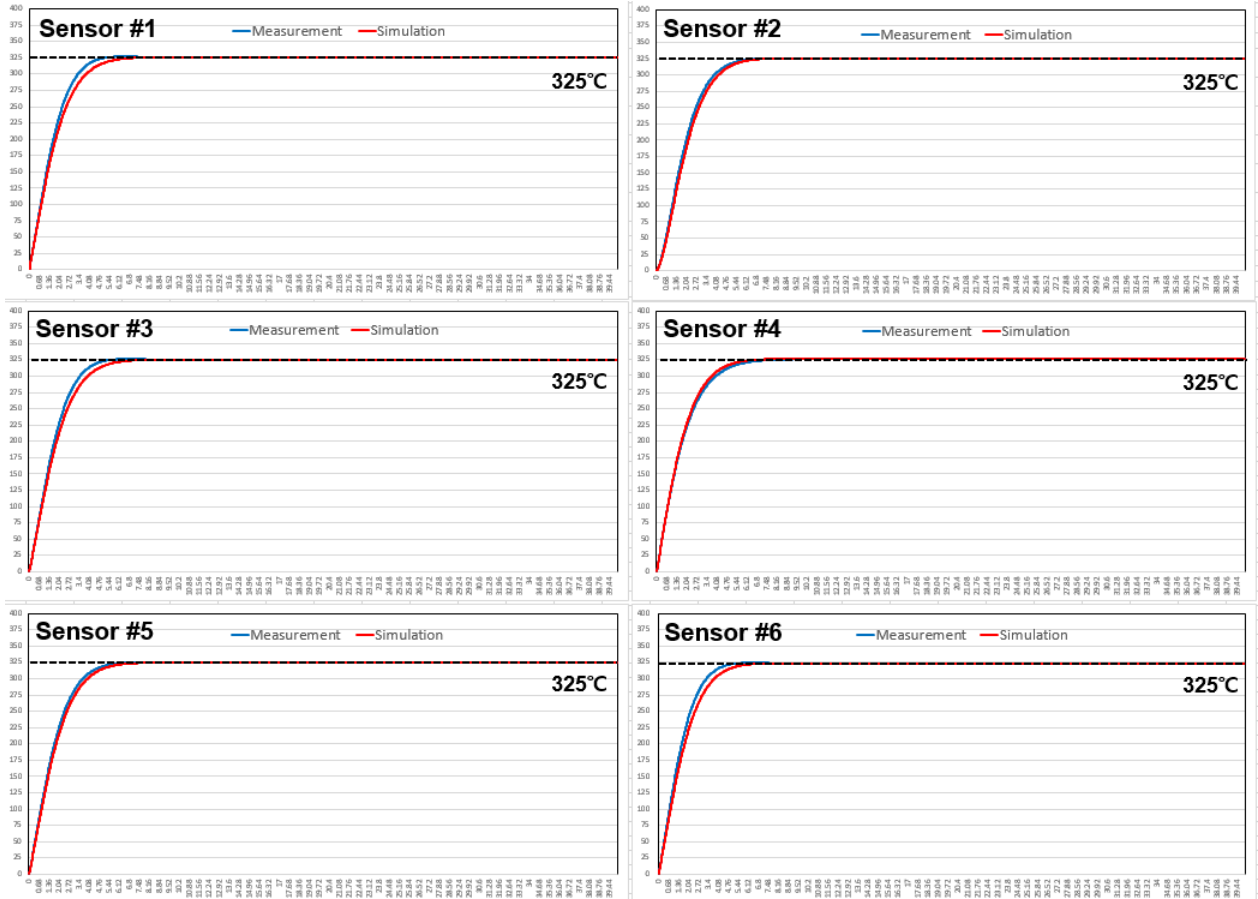
Figure 4.9 Measurement results of thermal transient response for actual µ-heater

And table 4.2 indicates the comparison of transient specifications between simulation results and measurement results. It can be represented that both of results are satisfying the desired transient specifications.

\

Table 4.2 The comparison of transient specifications between simulation and measurement results

Sensor	Simulation				Measurement				PM
	Tr	Ts	%OS	e_{ss}	Tr	Ts	%OS	e_{ss}	
#1	3.3m	5.4m	0.03%	0	2.9m	4.73m	0.07%	-0.10°C	50.2deg
#2	2.9m	5.2m	0.02%	0	2.7m	4.9m	0.03%	-0.91°C	48.6deg
#3	3.1m	5.1m	0.01%	0	2.8m	4.8m	0.02%	+0.12°C	52.7deg
#4	3.2m	4.9m	0.03%	0	3.3m	5.1m	0.02%	-1.27°C	49.3deg
#5	3.1m	5.2m	0.01%	0	2.9m	5.0m	0.06%	-0.05°C	51.9deg
#6	3.1m	5.1m	0.02%	0	2.7m	4.8m	0.10%	+0.37°C	50.5deg

V. CONCLUSION AND FUTURE WORK

From now on, temperature control system of gas sensor micro heater was dealt with. The optimal temperature for the best response of measured micro heater was 350°C and we saw that the feedback temperature value properly follows the set-point value with dynamic transient response which also satisfies the transient specifications. Now we need to look into the driving power dissipated in micro heater. First, let us look into figure 5.1 which indicates that the comparison of heater power consumption in low operating temperature. Red line shows the power consumption using continuous current driving method with current source. And blue line shows the power consumption using PWM current driving method with switching transistor. And the numbers with green color indicate power efficiency of PWM current driving method against with continuous current driving method. And the figure 5.2 also shows the comparison of two current driving method, however, it is operated in high operating temperature. As you see the power efficiency of figure 5.2, they show less efficient results than the one of figure 5.1. This is because when the heater temperature goes high, it need larger duty-on time. It means longer switch-on time of the transistor and it is difficult to achieve higher power efficiency in driving micro heater.
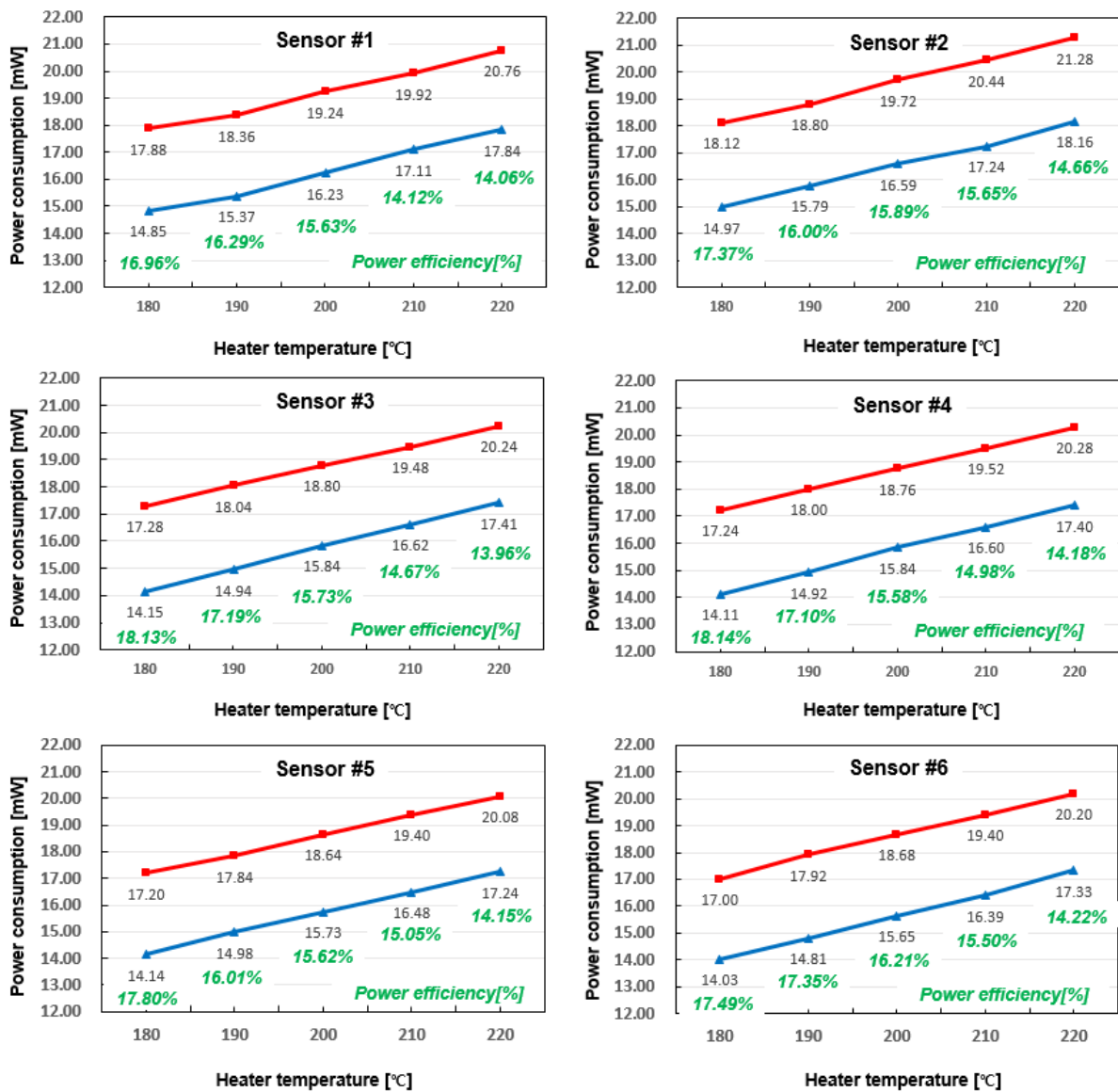
Figure 5.1. Power consumption comparison in low heater temperature between two current driving methods (Total power consumption[mW] vs Heater temperature[℃])

Red line: Continuous current driving method by current source;

Blue line: Pulse-width modulated current driving method by switching transistor
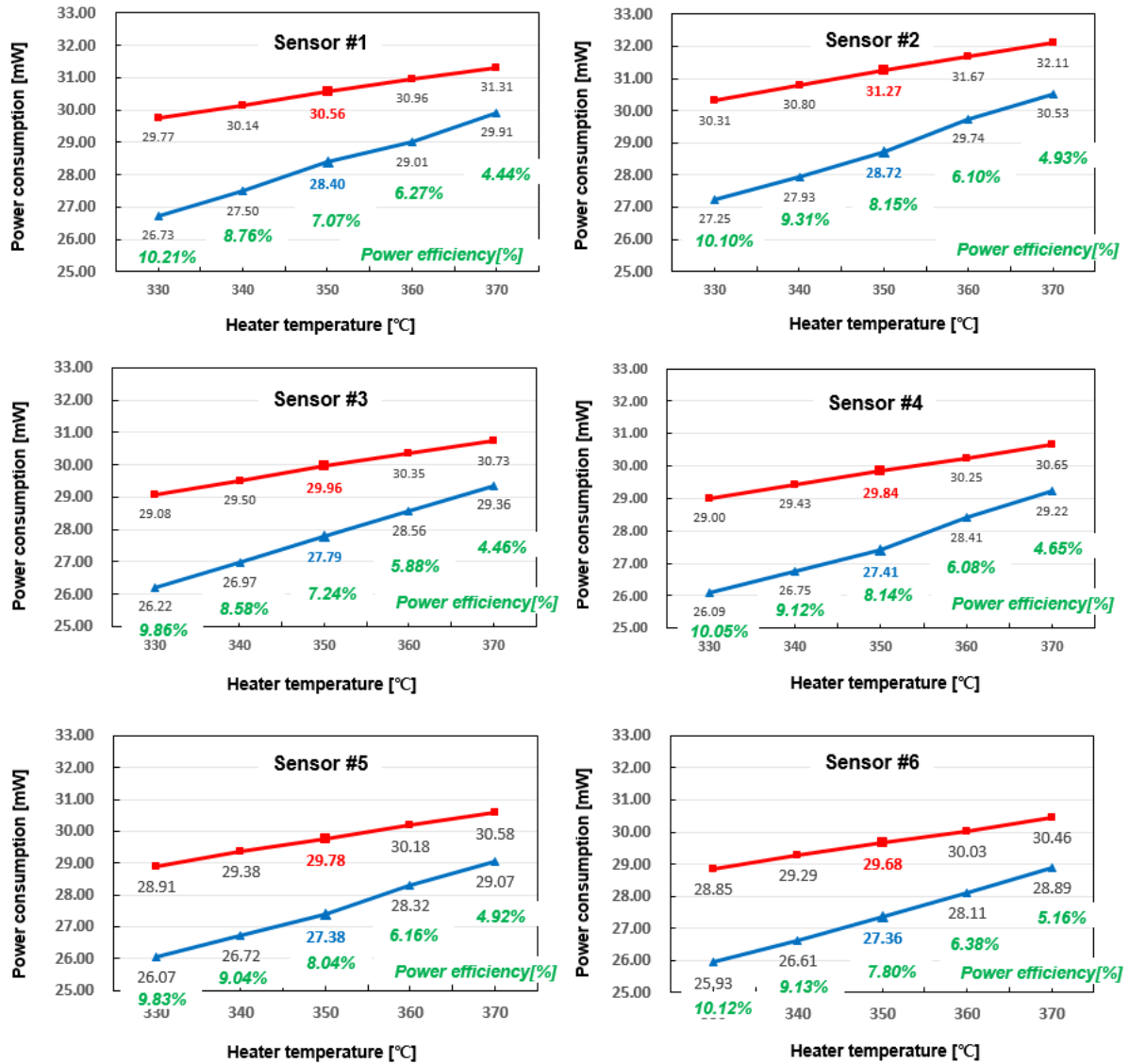
Figure 5.2. Power consumption comparison in high heater temperature between two current driving methods (Total power consumption[mW] vs Heater temperature[℃])

Red line: Continuous current driving method by current source;

Blue line: Pulse-width modulated current driving method by switching transistor

As a future work, additional measurement for driving micro heater will be conducted. And the driving circuits implemented in FPGA will be combined for ASIC. The approach for the system on one-chip can facilitate to the applications for the portable instruments.

References

[1] S. J. S. S. S. J. M.H.Kwon, "Indoor Air Polluion and Health Effects in Residential Apartment," National Institute of Environmental Research, Dec 2009.

[2] L. Y. L. Z. D. X. a. R. G. Chengxiang Wang, "Metal Oxide Gas Sensors: Sensitivity and Influencing Factors," *Sensors,* vol. 10, pp. 2088-2106, October 2010.

[3] M. G. W. H. S. K.-U. K. A. H. Diego Barrettino, "Hotplate_based Monolithic CMOS Microsystems for Gas Detection and Material Characterization for Operating Temperatures up to 500℃," *IEEE Journal of Solid-State Circuits,* vol. 39, no. 7, pp. 1202-1207, July 2004.

[4] M. G. S. T. S. H. C. H. A. H. Diego Barrettino, "CMOS Monolithic Metal-Oxide Gas Sensor Microsystems," *IEEE Sensors Journal,* vol. 6, no. 2, pp. 276-286, April 2006.

[5] P. S. S. M. E. F. V.Garofalo, "Mixed Signal Temperature Control Circuit for On-chip CMOS Gas Sensor," *International Semiconductor Conference,* vol. 2, pp. 495-498, 2009.

[6] N. M. e. a. I. Simon, "Micromachined Metal oxide Gas Sensors: Opportuniies to improve sensor performance," *Sensors and Acutators,* vol. 73, pp. 1-26, 2001.

[7] J. G.-V. A. T.-F. M. Alfredo Reyes-Barranca, "Thermal model for a microhot plate used in a MEM gas sensor," *REVISTA MEXICANAN DE FISICA,* vol. 54, pp. 15-24, June 2008.

[8] N. S. Nise, Control Systems Engineering, sixth Edition, International Student Version, John Wiley & Sons, Inc.

[9] "Control Tutorials for MATLAB and Simulink," [Online]. Available: http://ctms.engin.umich.edu/CTMS/index.php?aux=Activities_Lightbulb. [Accessed 26 July 2016].

[10] M. W. W. Yuen Fong Chan, "Design and Implementation of Modular FPGA-Based PID Controllers," *IEEE Transactions on Industrial Electronics,* vol. 54, no. 4, pp. 1898-1906, August 2007.

[11] R. V. M. V. A. A. S. J. Jain, "Implementation of a PID control PWM Module on Altera DE0 Kit Using FPGA," *IEEE First International Conference on Control, Measurement and Instrumenation (CMI),* pp. 341-345, 2016.

[12] "ADC101S101 Single Channel, 0.5 to 1Msps, 10-Bit A/D Converter," TEXAS INSTRUMENTS,

[Online]. Available: www.ti.com.

요약문

저전력 가스센서 마이크로 히터 동작 회로

반도체식 가스센서 내부에는 외부 가스를 감지하는 센싱부와 화학 반응이 가장 잘 반응하기에 필요한 열을 발생시키는 히터부로 이루어져 있다. 가스 센서가 높은 민감도를 가지기 위해선 마이크로 히터부에서 최적의 온도를 센싱부로 공급해주어야 한다. 또한, 모든 가스 센서의 최적의 히터 온도는 센싱부의 메테리얼과 타겟하는 가스마다 다르다. 따라서, 가스센서의 마이크로 히터의 온도를 조절할 수 있는 동작 회로를 필요로 하게 된다. 시스템의 동작 회로로 비례-적분 제어기와 펄스폭변조를 사용하였다. 비례-적분 제어기를 쓰면 높은 온도 정확도와 빠른 응답 특성을 얻을 수 있다. 펄스폭변조를 사용한 전류 동작 방법을 사용하면 지속적인 전류 동작 방법보다 더 낮은 전력을 소모할 수 있다. 지속적인 전류 동작 방법은 전력을 지속적으로 소모하는 반면 펄스폭변조를 사용하면 듀티가 온 이 되는 시간에만 소모하기 때문에 보다 높은 열적 효율을 얻을 수 있다. ADC 칩을 조절할 수 있는 ADC 인터페이스 블록을 설계하였다. 또한, 이 논문에서 이상적은 시스템 온도 응답 특성을 얻기 위한 비례-적분 게인 튜닝 방법을 소개한다.

동작 회로들은 Field-Programmable Gate Array(FPGA) 로 설계 하였고, 개발 보드로는 Altera Cyclone IV DE2-115 보드를, 논리 합성 툴과 RTL 시뮬레이션 툴로써 Altera Quartus II 와 Mentographics Modelsim 을 사용하였다. 측정에 사용된 가스센서 마이크로 히터는 연세대학교 기계공학과 김종백 교수님 연구실에서 제작된 모델을 사용하였고 모델링에 필요한 변수들에 대한 정보를 받아 진행하였다.